

JGR Atmospheres

RESEARCH ARTICLE

10.1029/2019JD030623

Key Points:

- First ever measurements with a high-accuracy single-particle soot photometer of black carbon (BC) concentrations in Arctic snowpack
- Topography and BC emission flux strongly influenced latitudinal variations of mass concentrations and size distributions of BC
- Measured BC mass concentrations 2–25 times lower than previously reported show the importance of revalidating climate models

Supporting Information:

- Supporting Information S1
- Table S1
- Table S2
- Table S3
- Table S4
- Table S5
- Table S6
- Table S7
- Table S8
- Table S9
- Table S10
- Table S11
- Table S12
- Table S13
- Table S14
- Figure S1
- Figure S2
- Figure S3
- Figure S4
- Figure S5
- Figure S6
- Figure S7
- Figure S8
- Figure S9
- Figure S10
- Figure S11
- Figure S12

Correspondence to:

T. Mori,
mori@rs.tus.ac.jp

Citation:

Mori, T., Goto-Azuma, K., Kondo, Y., Ogawa-Tsukagawa, Y., Miura, K., Hirabayashi, M., et al. (2019). Black carbon and inorganic aerosols in Arctic snowpack. *Journal of Geophysical Research: Atmospheres*, 124, 13,325–13,356. <https://doi.org/10.1029/2019JD030623>

Received 14 MAR 2019







Accepted 22 OCT 2019

Accepted article online 7 NOV 2019

Published online 14 DEC 2019

©2019. American Geophysical Union.
All Rights Reserved.

Black Carbon and Inorganic Aerosols in Arctic Snowpack

Tatsuhiko Mori¹ , Kumiko Goto-Azuma^{2,3}, Yutaka Kondo² , Yoshimi Ogawa-Tsukagawa², Kazuhiko Miura¹, Motohiro Hirabayashi², Naga Oshima⁴, Makoto Koike⁵ , Kaarle Kupiainen⁶, Nobuhiro Moteiki⁵ , Sho Ohata^{7,8}, P.R. Sinha⁹, Konosuke Sugiura¹⁰, Teruo Aoki¹¹ , Martin Schneebeli¹² , Konrad Steffen¹², Atsushi Sato¹³, Akane Tsushima¹⁴, Vladimir Makarov¹⁵, Satoshi Omiya^{16,17}, Atsuko Sugimoto¹⁸, Shinya Takano¹⁸, and Naoko Nagatsuka²

¹Department of Physics, Faculty of Science Division I, Tokyo University of Science, Tokyo, Japan, ²National Institute of Polar Research, Tachikawa, Japan, ³The Graduate University for Advanced Studies, Hayama, Japan, ⁴Meteorological Research Institute, Tsukuba, Japan, ⁵Department of Earth and Planetary Science, Graduate School of Science, The University of Tokyo, Tokyo, Japan, ⁶Finnish Environment Institute, Helsinki, Finland, ⁷Institute for Space–Earth Environmental Research, Nagoya University, Nagoya, Japan, ⁸Institute for Advanced Research, Nagoya University, Nagoya, Japan, ⁹Department of Earth and Space Sciences, Indian Institute of Space Science and Technology, Thiruvananthapuram, India, ¹⁰Department of Earth System Science, Faculty of Sustainable Design, University of Toyama, Toyama, Japan, ¹¹Graduate School of Natural Science and Technology, Okayama University, Okayama, Japan, ¹²WSL Institute for Snow and Avalanche Research, Davos, Dorf, Switzerland, ¹³Snow and Ice Research Center, Nagaoka, Japan, ¹⁴Research Institute for Humanity and Nature, Kyoto, Japan, ¹⁵Melnikov's Permafrost Institute, Yakutsk, Russia, ¹⁶Institute of Low Temperature Science, Hokkaido University, Sapporo, Japan, ¹⁷Civil Engineering Research Institute for Cold Region, Sapporo, Japan, ¹⁸Graduate School of Environmental Science, Hokkaido University, Sapporo, Japan

Abstract Black carbon (BC) deposited on snow lowers its albedo, potentially contributing to warming in the Arctic. Atmospheric distributions of BC and inorganic aerosols, which contribute directly and indirectly to radiative forcing, are also greatly influenced by depositions. To quantify these effects, accurate measurement of the spatial distributions of BC and ionic species representative of inorganic aerosols (ionic species hereafter) in snowpack in various regions of the Arctic is needed, but few such measurements are available. We measured mass concentrations of size-resolved BC (C_{MBC}) and ionic species in snowpack by using a single-particle soot photometer and ion chromatography, respectively, over Finland, Alaska, Siberia, Greenland, and Spitsbergen during early spring in 2012–2016. Total BC mass deposited per unit area (DEP_{MBC}) during snow accumulation periods was derived from C_{MBC} and snow water equivalent (SWE). Our analyses showed that the spatial distributions of anthropogenic BC emission flux, total precipitable water, and topography strongly influenced latitudinal variations of C_{MBC} , BC size distributions, SWE, and DEP_{MBC} . The average size distributions of BC in Arctic snowpack shifted to smaller sizes with decreasing C_{MBC} due to an increase in the removal efficiency of larger BC particles during transport from major sources. Our measurements of C_{MBC} were lower by a factor of ~13 than previous measurements made with an Integrating Sphere/Integrating Sandwich spectrophotometer due mainly to interference from coexisting non-BC particles such as mineral dust. The SP2 data presented here will be useful for constraining climate models that estimate the effects of BC on the Arctic climate.

Plain Language Summary Black carbon (BC) particles, commonly known as soot, are emitted from incomplete combustion of fossil fuels and biomass. They efficiently absorb solar radiation and thus heat the atmosphere. BC particles emitted at midlatitudes and in the Arctic are deposited onto snow in the Arctic, accelerating snowmelt in early spring by absorbing solar radiation. These processes contribute to warming in the Arctic. Calculations of this warming effect by using numerical models need to be validated by comparison with observed BC concentrations in snowpack. However, there are very few accurate records of concentrations of BC in snow because of technical difficulties in making these measurements. We developed a new laser-induced incandescence technique to measure BC concentrations in snowpack and applied it for the first time in six Arctic regions (Finland, Alaska, North and South Siberia, Greenland, and Spitsbergen). The BC concentrations we measured were highest in Finland and South Siberia, which are closer to large anthropogenic BC sources than the other regions, where our measured BC concentrations were much lower. On average, our BC concentrations were much lower than those previously measured by different techniques. Therefore, previous comparisons of modeled and observed BC concentrations need to be re-evaluated using the present data.

1. Introduction

Black carbon (BC) particles, emitted at midlatitudes and in the Arctic, are transported over long distances during which BC particles are removed by both dry and wet deposition processes (AMAP, 2015; Bond et al., 2013; Browse et al., 2012; Liu et al., 2015). These particles efficiently absorb solar radiation and thus heat the atmosphere (Bond et al., 2013). The absorption of sunlight by BC particles deposited onto snow in the Arctic accelerates snowmelt and reduces snow albedo, contributing to warming near the Earth's surface (Bond et al., 2013; Flanner et al., 2007; Hadley & Kirchstetter, 2012). However, there are large uncertainties in climate-model estimates of the effect of BC on snow albedo because of uncertainties in the prediction of key parameters (mass and number size distributions of BC in surface snow and the total column of snowpack, and amounts of BC deposition by mass and number in the total column of snowpack). Therefore, measurement of these parameters is of critical importance for modeling that aims to quantify the effects of BC deposition on snow albedo. However, very few accurate measurements of BC in snowpack have been made, due partly to technical difficulties, as detailed below.

Mass concentrations of BC in snow (C_{MBC}) in Arctic regions, including Alaska, Canada, Greenland, Svalbard, mainland Norway, Russia, and the Arctic Ocean have been measured mainly by the Integrating Sphere/Integrating Sandwich spectrometer (ISSW) method (Doherty et al., 2010). In this method, C_{MBC} (ISSW) is estimated from spectrally resolved measurements of the absorption coefficient of solid particles collected on a filter, by assuming a unitary absorption Ångström exponent for BC and associating most long-wavelength (650–700 nm) absorption to BC. However, these techniques have large measurement uncertainties attributed mainly to interference from coexisting non-BC solid particles, such as mineral dust, and filter undercatch (Doherty et al., 2010, 2016; Schwarz et al., 2012). C_{MBC} has also been measured by the thermal-optical transmittance (TOT) method (Aamaas et al., 2011; Forsström et al., 2009, 2013), although this technique has been reported to be unreliable (Lim et al., 2014).

Thus far, C_{MBC} determined by climate models has been compared mainly with C_{MBC} (ISSW) data from the Arctic (Dou et al., 2012; Jiao et al., 2014; Lee et al., 2013). Therefore, accurately measured C_{MBC} data are essential to validate climate models because the large uncertainties of C_{MBC} (ISSW) data have cast serious doubt on the validity of these comparisons.

To accurately measure the size distributions of BC in snow in this study, we used a single-particle soot photometer (SP2) based on a laser-induced incandescence technique, combined with a nebulizer (Kaspari et al., 2011; Lim et al., 2014; McConnell et al., 2007; Mori et al., 2016; Sinha et al., 2018; Wendl et al., 2014). The nebulizer/SP2 system has been used to measure the size distribution of BC in snow at Alert in Nunavut, Canada, and at Ny-Ålesund, Woodfjorden, and Mine in Spitsbergen, Norway (Khan et al., 2017; Macdonald et al., 2017; Sinha et al., 2018). In particular, Sinha et al. (2018) investigated the seasonal progression of deposition of BC by snowfall at Ny-Ålesund.

In this study, we applied the nebulizer/SP2 technique to snowpack in wider regions of the Arctic to derive the mass concentrations and number concentrations of BC (C_{MBC} and C_{NBC}), the size distribution of BC in snowpack, and the deposition amount per unit area (DEP) of BC by mass and by number (DEP_{MBC} and DEP_{NBC} , respectively) during snow accumulation periods.

It is well known that inorganic aerosols contribute directly and indirectly to negative radiative forcing (Intergovernmental Panel on Climate Change, 2013; Lohmann & Feichter, 2005; Yu et al., 2006). Measurement of the concentrations of inorganic aerosols in snowpack in the Arctic is also important for understanding the process of their deposition. The deposition process is a key control on their concentrations in the atmosphere. Some measurements of nonsea-salt sulfate ($nss\text{-SO}_4^{2-}$) and NO_3^- concentrations in snowpack have been made in Arctic regions including Scandinavia, Alaska, Canada, and Norway (Douglas & Sturm, 2004; Macdonald et al., 2017; Raidla et al., 2015; Wright & Dovland, 1978), but the spatial distribution of these measurements is limited. Because of the scarcity of these data, we measured mass concentrations of ionic species representative of inorganic aerosols ($nss\text{-SO}_4^{2-}$ ($C_{nss\text{-SO}_4^{2-}}$), NO_3^- ($C_{\text{NO}_3^-}$), NH_4^+ ($C_{\text{NH}_4^+}$), and Na^+ (C_{Na^+})) in snowpack together with C_{MBC} . We also measured the DEP of these ions ($DEP_{nss\text{-SO}_4^{2-}}$, $DEP_{\text{NO}_3^-}$, $DEP_{\text{NH}_4^+}$, and DEP_{Na^+}).

We have characterized the deposition of size-resolved BC particles and inorganic aerosol ion species (ionic species hereafter) by accurately measuring their concentrations in snow samples collected from six regions

Table 1
Definitions of Parameters Used in This Study

Parameter	Unit	Definition
D_{BC}	nm	Diameter of BC core
C_{MBC}	$\mu\text{g/L}$	BC mass concentration in snowpack
C_{NBC}	$1/\mu\text{L}$	BC number concentration in snowpack
C_{ion}	$\mu\text{eq/L}$	Concentrations of ionic species (nonsea-salt sulfate nss-SO_4^{2-} , NO_3^- , Na^+ , and NH_4^+) in snowpack
SWE	mm	Snow water equivalent
DEP_{MBC}	$\mu\text{g/m}^2$	Deposition amount of BC by mass in total column of snowpack during snow accumulation period
DEP_{NBC}	$1/\text{m}^2$	Deposition amount of BC by number in total column of snowpack during snow accumulation period
DEP_{ion}	$\mu\text{eq/m}^2$	Deposition amount of ionic species (nss-SO_4^{2-} , NO_3^- , Na^+ , and NH_4^+) in total column of snowpack during snow accumulation period
EF_{BC}	$\text{ng m}^{-2} \text{ s}^{-1}$	Anthropogenic BC emission flux
MMD	nm	Mass median diameter for BC mass size distribution
CMD	nm	Count median diameter for BC number size distribution
σ_{gm}		Geometric standard deviations for BC mass size distributions
σ_{gc}		Geometric standard deviations for BC number size distributions
f_{600}		Ratio of the cumulative mass concentration of BC integrated from 600 to 4,170 nm to total C_{MBC}
m_{BC}	fg	Mass per BC particle (C_{MBC}/C_{NBC})
RH	%	Relative humidity, obtained from NCEP/NCAR global reanalysis data
w	g/kg	Water vapor mixing ratio, estimated from NCEP/NCAR global reanalysis data
TPW	kg/m^2	Total precipitable water, estimated from NCEP/NCAR global reanalysis data
MAC	m^2/g	Mass absorption cross section of BC

of the Arctic (Finland, Alaska, North and South Siberia, Greenland, and Spitsbergen) in early spring during 2012–2016. To interpret these data, we used meteorological data (temperature, relative humidity, and wind), snow water equivalent (SWE), BC emission inventories, and topographic data. These data allowed us to systematically investigate the variability of concentrations of BC and inorganic aerosol ions in Arctic snowpack. Terminologies used in this study are summarized in Table 1.

2. Methods

2.1. Collection of Snow Samples

We collected snow in Finland, Alaska, North and South Siberia, Greenland, and Spitsbergen in early spring during 2012–2016 (Figure 1a). In total, we collected 107 samples of surface snow (0–2- or 0–5-cm depth), 77 samples of subsurface snow (2–10 cm), and 112 total columns of snowpack. The number of snow samples is summarized for each region in Table 2. In all areas except North Siberia and Greenland, columns of snowpack were collected from the snow surface to near the ground surface when snow depths had reached their approximate maxima between February and April, before the start of snowmelt (see section 3). In Spitsbergen, snow pits were dug and samples were collected from the pit walls. In other regions, samples were collected by using an acrylic tube sampler. The columns of snowpack therefore represent total accumulated snow from the beginning of the snow cover period until the day of collection. In North Siberia and Greenland, most of the snow samples were collected in April and May, respectively.

To minimize local anthropogenic effects, sampling sites were chosen to avoid densely populated areas and roads. To avoid contamination during sampling, a stainless-steel spatula (Doherty et al., 2010; Sinha et al., 2018; Tollefson, 2009) was used to collect samples in powder-free plastic bags (Igarashi Kasei, Co., Ltd., Tokyo, Japan). Snow samples were then melted and stirred in their bags, and portions of melted samples from each bag were transferred into precleaned glass bottles for BC analyses and polypropylene bottles for ionic species analyses. These samples were transported by air freight to the National Institute of Polar Research (NIPR) in Japan. Until analysis, the samples in glass bottles for BC were kept in a refrigerator at 4 °C and those in polypropylene bottles for ionic species were kept in a freezer at –20 °C or –30 °C. The storage periods of the melted snow samples are summarized for each region in Table 3.

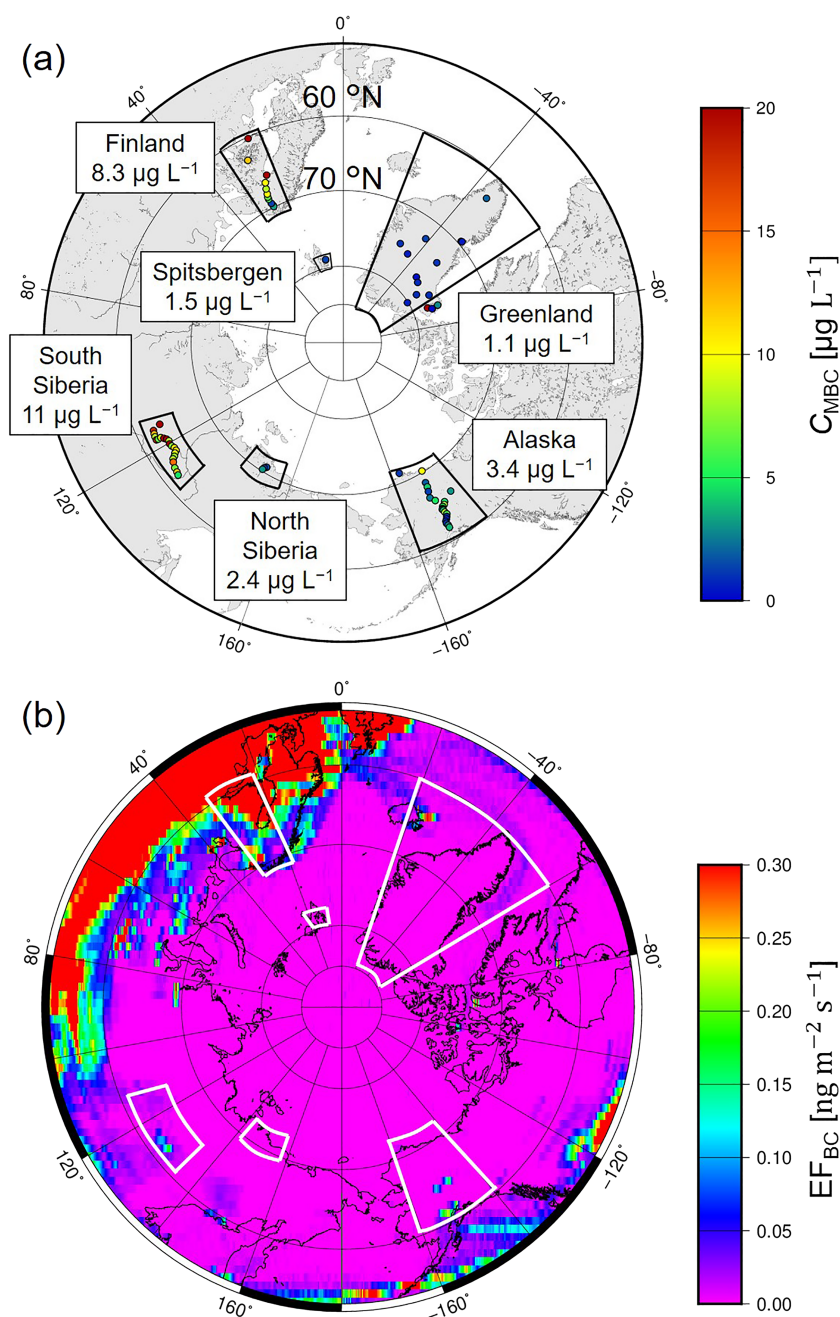


Figure 1. Maps of the Northern Hemisphere showing (a) locations of snow samples used in this study and median values of BC mass concentrations in snowpack (C_{MBC}) for each of the regions studied and (b) average annual anthropogenic BC emission flux (EF_{BC}) at a horizontal resolution of 0.5° lat/long from MACCity (MACC/CityZEN EU projects) emission data for 2013.

Snow density was determined in the field from the mass of each sample and the volume of the sampler used. A stainless-steel snow sampler (100 cm^3) was used for surface samples and an acrylic tube sampler (cross sectional area of 50 cm^2) was used for columns of snowpack. The snow depth was also directly measured.

SWE (mm) is a key parameter to estimate DEP of BC and ionic species in snowpack from the beginning of the snow cover period until the day of collection, and it was calculated as the product of snow depth and snow density. However, DEP values for surface snow samples were not determined because of difficulties in accurate measurement of surface snow density.

Table 2
Details of Snow Sampling Programs

Region	Year	Number of sites	Number and type of snow samples		
			Column	Surface	Subsurface
Finland	2013	11	11	-	-
Alaska	2012	15	15	-	-
	2013	14	19	18	17
	2014	13	13	13	13
	2015	11	28	26	20
Siberia (South)	2013	24	24	-	-
Siberia (North)	2015	5	-	5	-
Greenland	2012	1	-	8	5
	2013	4	-	10	3
	2014	8	-	8	-
	2015	7	-	9	9
	2016	8	-	8	8
Ny-Ålesund	2013	2	2	2	2

2.2. Emission Flux of BC

According to data from MACC/CityZEN EU projects (<https://eccad3.sedoo.fr/>; Lamarque et al., 2010), the year-to-year variability of annual average anthropogenic emission flux of BC (EF_{BC}) was very low during our study period (2012–2016; see Figure 1b for EF_{BC} data for 2013). We used the EF_{BC} data to interpret the distributions of BC particles deposited onto snow during our study period (discussed in sections 4 and 5). It is likely that the column amounts of ambient BC in the lower troposphere greatly influence C_{MBC} , although the altitude that controls C_{MBC} varies with meteorological conditions (Mori et al., 2014). Observations at Hedo in Japan, downstream of the Asian continent, have shown that monthly average C_{MBC} in rainwater is correlated with near-surface ambient BC mass concentrations (Mori et al., 2014). However, there have been no comparable observational studies in the Arctic that directly link ambient BC and C_{MBC} . In this study, we investigated the relationship between C_{MBC} and EF_{BC} by assuming that ambient BC concentrations are generally related to the distributions of EF_{BC} (i.e., intensities of emissions and the distances between emitting regions and our snow sampling regions).

We did not use wildfire BC emission data, obtained from satellite measurements, because Northern Hemisphere wildfire emissions from winter to early spring during 2012–2016 were negligibly small (Rémy et al., 2017).

2.3. Measurement of BC in Snow

Techniques for accurately measuring C_{MBC} and C_{NBC} in water are described in detail elsewhere (Katich et al., 2017; Mori et al., 2016; Moteki & Mori, 2015; Sinha et al., 2018). In brief, we sonicated melted snow samples in an ultrasonic bath for 15 min to remove BC particles attached to the glass walls of the sample bottles (Mori et al., 2014). Each sample was then injected into a concentric pneumatic nebulizer (Marin-5; Cetac Technologies Inc., Omaha, Nebraska, USA) by a peristaltic pump (REGLO Analog; ISMATEC SA, Feldeggstrasse, Glattbrugg, Switzerland) at a constant flow rate of 3.2×10^{-6} L/s. The introduced water was converted to small droplets (2–3- μ m diameter) by the nebulizer and evaporated in the spray chamber heated to 140 °C to generate airborne particles, including BC particles, and water vapor. Some of the water vapor was removed through the first drain lines in the Marin-5, together with some aerosols. The remaining water vapor was condensed at 2 °C and then removed through other drain lines. The extracted BC particles were introduced into an SP2 at a constant gas flow rate of 15.2 cm³/s at standard temperature and pressure.

Table 3
Sample Storage Periods for Each Region

Region	Year sampled	Sample storage period
Finland	2013	15 months
Alaska	2012	27 months
Alaska	2013	15 months
Alaska	2014	3 months
Alaska	2015	1 month
South Siberia	2013	15 months
North Siberia	2015	1 month
Greenland	2012	27 months
Greenland	2013	16 months
Greenland	2014	3 months
Greenland	2015	9 months
Greenland	2016	21 months
Ny-Ålesund	2013	13 month

In general, SP2 detects incandescence emitted from individual light-absorbing particles in two wavelength bands (blue and red bands). Because the measured blue- and red-band incandescence signal ratios are related to the vaporization temperatures of light-absorbing particles, BC particles are clearly separated from other light-absorbing particles (i.e., dust; Moteki & Kondo, 2010; Yoshida et al., 2016). Schwarz et al. (2012) demonstrated that the size distributions of BC in dust-contaminated samples are not significantly affected by the presence of dust. Thus, the effect of interference of non-BC light-absorbing particles on BC data is very small.

The detectable mass equivalent diameter of BC (D_{BC}) has previously been determined by an SP2 to be 70 to 600 nm (Lim et al., 2014). In this study, we expanded the upper limit of detectable BC size to about 4,170 nm by using the method of Mori et al. (2016) to modify the photodetector to measure a larger incandescence signal and assuming a BC density of 1.8 g/cm³ with an uncertainty of 5% (Moteki et al., 2010; Moteki & Kondo, 2010). To determine the masses of individual BC particles, we used the relationship

between peak incandescence signal and BC mass for fullerene soot samples up to 320 nm. For larger BC diameters (>320 nm), the relationship was extrapolated to diameters up to 4,170 nm (Mori et al., 2016).

C_{MBC} ($\mu\text{g/L}$) was derived as follows:

$$C_{\text{MBC}}(D_{\text{BC}}) = \frac{F_{\text{neb}}}{V_{\text{pump}}} \int_{70}^{4170} \frac{dM_{\text{BC}}}{\epsilon(D_{\text{BC}}) d\log D_{\text{BC}}} d\log D_{\text{BC}}, \quad (1)$$

where $dM_{\text{BC}}/d\log D_{\text{BC}}$ is the measured size-resolved BC mass concentration in air ($\mu\text{g/m}^3$), F_{neb} is the nebulizer gas flow rate (cm^3/s), V_{pump} is the liquid flow rate of the peristaltic pump (L/s), and ϵ is the extraction efficiency of the Marin-5 nebulizer. C_{NBC} ($1/\mu\text{L}$) was also derived from the size-resolved BC number concentration in air ($1/\text{cm}^3$) and ϵ . The value of ϵ for the Marin-5 nebulizer was stable at about $50 \pm 4\%$ for $D_{\text{BC}} < 2,000$ nm and gradually decreased for $D_{\text{BC}} > 2,000$ nm (Katich et al., 2017; Mori et al., 2016; Moteki & Mori, 2015; Sinha et al., 2018). These C_{MBC} and C_{NBC} were derived by measuring more than 20,000 BC particles from each snow sample. The overall accuracy of the measured BC concentrations in water was about 16% (Mori et al., 2016).

The Marin-5/SP2 technique has been shown by theoretical and experimental studies to be reliable for measurement of size-resolved C_{MBC} and C_{NBC} in rainwater (Mori et al., 2016; Moteki & Mori, 2015). There are three main advantages in the use of this technique (Mori et al., 2016; Moteki & Mori, 2015): (1) BC size and C_{MBC} are stable during periods of storage in water, (2) the effect of coagulation of BC particles during extraction by the nebulizer is negligible for water samples with $C_{\text{MBC}} < 64 \mu\text{g/L}$, and (3) the Marin-5 nebulizer can stably extract particles up to 2,000-nm diameter with a size-independent extraction efficiency of $\sim 50\%$.

2.4. Reproducibility of C_{MBC} in Snow Samples

Our melted snow samples were refrigerated at 4°C for periods ranging from 1 to 27 months before analysis (Table 3). We investigated any temporal changes of BC size distributions in eight samples melted from a single Greenland ice core. The first measurements, immediately after melting (day 1), produced C_{MBC} from 0.4 to $1.6 \mu\text{g/L}$ and C_{NBC} from 70 to $320 /\mu\text{L}$. The shapes of the mass and number size distributions of BC of the same samples analyzed 10 months later changed little, as shown in Figures 2a and 2b, as a typical example. In this case, the C_{MBC} and C_{NBC} values agreed to within 5.6% and 4.4%, respectively. Both C_{MBC} and C_{NBC} for all snow samples on day 1 and 10 months later were well correlated ($r^2 = 0.79$ for C_{MBC} and $r^2 = 0.87$ for C_{NBC}). The pairs of measurements of C_{MBC} and C_{NBC} agreed to within 5% and 8%, respectively (Figure 3). The $C_{\text{MBC}}(10 \text{ months})/C_{\text{MBC}}(\text{day 1})$ and $C_{\text{NBC}}(10 \text{ months})/C_{\text{NBC}}(\text{day 1})$ ratios for all the samples deviated from unity within $\pm 15\%$ and $\pm 20\%$, respectively, where $C_{\text{MBC}}(t)$ and $C_{\text{NBC}}(t)$ are the values measured at time t after melting. Moreover, changes of mass median diameter (MMD), count median diameter (CMD), and geometric standard deviations (σ_{gm} and σ_{gc}) for the mass and number size distributions over the 10-month period were negligibly small (not shown).

We also evaluated the reproducibility of the measured BC size distributions in 14 snowpack samples collected at Ny-Ålesund in 2013, using measurements made 13 and 42 months after the samples were melted. The C_{MBC} (13 months) values ranged from 0.8 to $5.0 \mu\text{g/L}$ and the C_{NBC} (13 months) values ranged from 200 to $1,000 /\mu\text{L}$. The mass and number size distributions of BC from the same samples had very similar shapes, as shown in Figures 2c and 2d. In this case, C_{MBC} (42 months) agreed with C_{MBC} (13 months) to within 3% and C_{NBC} (42 months) agreed with C_{NBC} (13 months) to within 7%. For all snowpack samples, the C_{MBC} (42 months)/ C_{MBC} (13 months) and C_{NBC} (42 months)/ C_{NBC} (13 months) ratios were 0.89 ± 0.21 and 0.80 ± 0.22 , respectively, on average ($r^2 = 0.78$ for C_{MBC} and $r^2 = 0.66$ for C_{NBC} ; not shown). Moreover, MMD, CMD, σ_{gm} , and σ_{gc} in all the snowpack samples agreed to within 9%, 2%, 6%, and 3%, respectively, on average.

A similar evaluation was made for two snowpack samples collected near Fairbanks, Alaska. In these samples, C_{MBC} (five months) agreed with C_{MBC} (one month) to within 12% and C_{NBC} (five months) agreed with C_{NBC} (one month) to within 1.0%, on average, with little change in MMD, CMD, σ_{gm} , and σ_{gc} .

These results demonstrate that C_{MBC} and C_{NBC} in melted snow samples from different sites with different concentrations were stable, to within about 20%, for 42 months after the first melt.

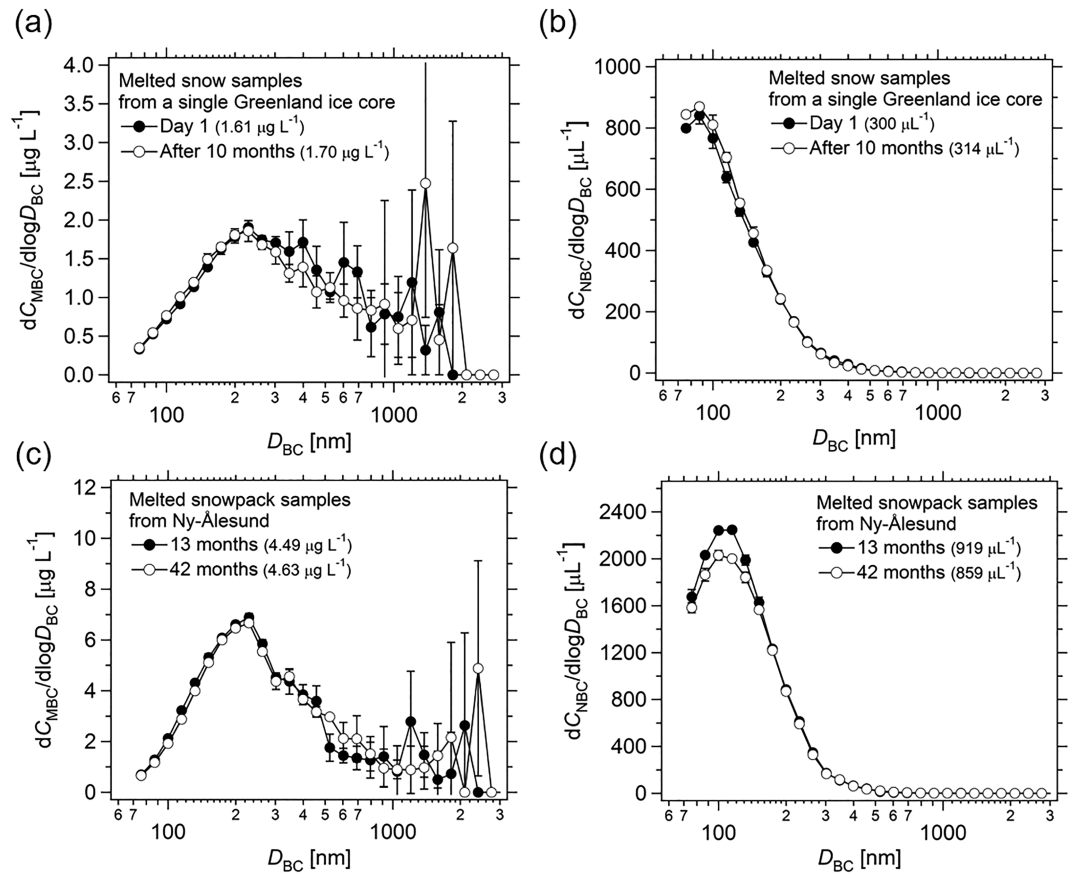


Figure 2. (a) Mass and (b) number size distributions of BC in melted snow samples from an ice core in Greenland, measured immediately after melting (day 1) and 10 months later. (c and d) Same as (a) and (b) but for snowpack samples from Ny-Ålesund, made 13 and 42 months after the samples were melted. Bars indicate $\pm 1\sigma$ values of a Poisson distribution.

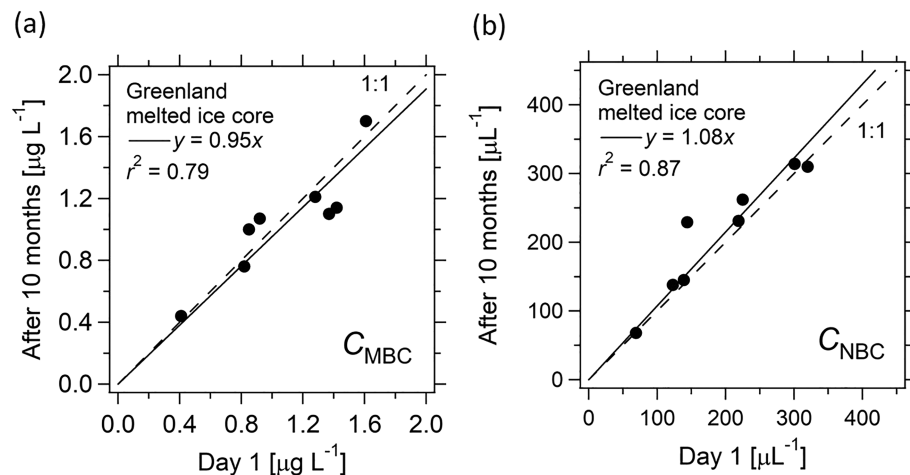


Figure 3. (a) Correlation between C_{MBC} of melted snow samples from an ice core in Greenland measured on day 1 and those measured 10 months later. (b) Same as (a) but for C_{NBC} . The solid lines indicate the least squares fitted regression.

2.5. Effects of BC Loss Due to Adhesion on Walls of Glass Bottles and Plastic Bags

We evaluated possible losses of BC due to its adhesion on the inner walls of sampling bags and glass bottles. Appendix A1 demonstrates that BC losses due to adhesion on the inner walls of the bags and glass bottles were small.

The results given in sections 2.3–2.5 demonstrate the overall high accuracy of our measurements of size-resolved C_{MBC} and C_{NBC} in snowpack, without interference by aerosols other than BC.

2.6. Size Distribution of BC

To characterize the size distributions of BC, we used two parameters: (1) the ratio of the cumulative mass concentration of BC integrated from 600 to 4,170 nm to total C_{MBC} ($70 \text{ nm} < D_{BC} < 4,170 \text{ nm}$), denoted as f_{600} , and (2) the mass per BC particle m_{BC} (C_{MBC}/C_{NBC} ; Moteki et al., 2012; Sinha et al., 2018). The correlation of f_{600} and m_{BC} for all areas sampled was strong ($r^2 = 0.75$; Figure A1). The choice of 600 nm is arbitrary to some extent because other diameters can be used as thresholds (e.g., 800 nm (f_{800}) and 1,000 nm (f_{1000})). In fact, f_{600} for all snow samples were positively correlated with f_{800} ($r^2 = 0.95$) and f_{1000} ($r^2 = 0.91$). Both of these parameters (f_{600} and m_{BC}) are useful to represent the average mass size distribution of BC by a single number, in addition to MMD, CMD, σ_{gm} , and σ_{gc} .

2.7. Deposition Amount of BC

The mass of BC deposited per unit area during snow accumulation periods, denoted as DEP_{MBC} ($\mu\text{g}/\text{m}^2$), was derived from C_{MBC} ($\mu\text{g}/\text{L}$) and SWE (mm) for each total column of snowpack as

$$DEP_{MBC} = C_{MBC} \times \text{SWE}. \quad (2)$$

The total number of BC particles deposited per unit area during the same period (DEP_{NBC}) was similarly derived from C_{NBC} .

2.8. Ionic Species

The concentrations of soluble ionic species SO_4^{2-} , NO_3^- , Na^+ , and NH_4^+ were measured by ion chromatography after frozen samples were melted at room temperature (Goto-Azuma et al., 2019). The samples collected during 2012–2014 were measured with DX-500 ion chromatographs (Dionex Corp., Sunnyvale, CA, USA), whereas those collected in 2015 and 2016 were measured with ICS-5000 ion chromatographs (Thermo Fisher Scientific Inc, Cambridge, MA, USA). IonPac AS11-HC and IonPac CS14 columns were used for anions and cations, respectively. As eluents, KOH and methane sulfonic acid were used for anions and cations, respectively. $C_{\text{nss-SO}_4^{2-}}$ was derived from the concentrations of SO_4^{2-} and Na^+ by assuming a $\text{SO}_4^{2-}/\text{Na}^+$ mass ratio in seawater of 0.12 (Keene et al., 1986). DEP values for the soluble ionic species were derived by adapting equation 2 for that purpose.

3. Meteorological Data

We obtained temperature and precipitation recorded at automated weather stations (AWS) in Finland (Irannezhad et al., 2014), Alaska (Leeper et al., 2015), Greenland (Steffen & Box, 2001), and Spitsbergen (Førland & Hanssen-Bauer, 2000) from the Finnish Meteorological Institute (<http://en.ilmatieteenlaitos.fi/>), Alaskan Climate Research Center (<http://akclimate.org/>), Greenland Climate Network (<http://cires1.colorado.edu/science/groups/steffen/gcnet/>), and Norwegian Meteorological Institute (http://sharki.oslo.dnmi.no/portal/page?_pageid=73,39035,73_39049&_dad=portal&_schema=PORTAL), respectively. Each of these AWSs was within about 5 km of our snow sampling sites. Continuous measurements of snow depths, based on a sonic sensor, were also conducted at AWSs in Finland, Alaska, and Spitsbergen.

We obtained vertical profiles of meteorological parameters (pressure, temperature, relative humidity (RH), wind speed, and wind direction) routinely measured at 0000 and 1200 UTC at several radiosonde stations in Finland, Alaska, South Siberia, Greenland, and Spitsbergen from the Integrated Global Radiosonde Archive (Durre et al., 2006), produced by the National Climatic Data Center (<https://www.ncdc.noaa.gov/data-access/weather-balloon/integrated-global-radiosonde-archive>). Each of these stations was within about 3 km of our snow sampling sites (see Figure A2 for example profiles). We used these profiles to estimate the height of the planetary boundary layer (PBL) near each snow sampling site (Appendix A2, Figure A3).

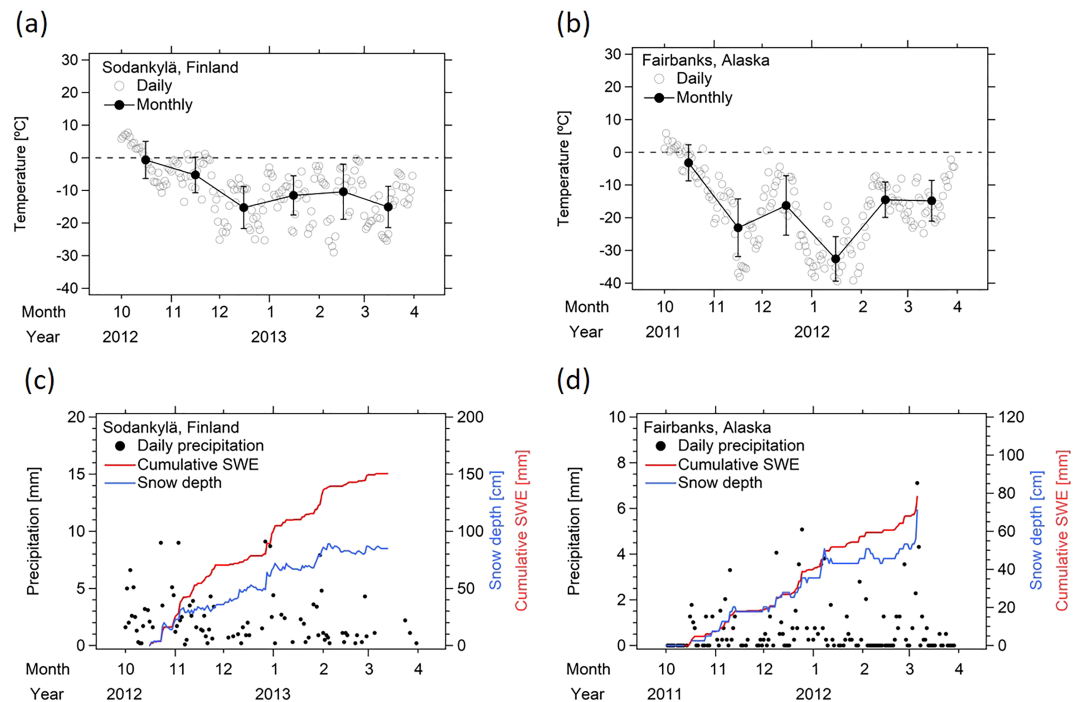


Figure 4. Daily and monthly average temperatures in (a) Sodankylä (Finland) from October 2012 to March 2013 and in (b) Fairbanks (Alaska) from October 2011 to March 2012, and daily precipitation and cumulative SWE and snow depth from the onset of snowfall to date of sampling in (c) Sodankylä and (d) Fairbanks. Error bars indicate $\pm 1\sigma$.

3.1. Temperature and Snowmelt

Figures 4a and 4b show examples of daily and monthly average air temperatures from October to March at Sodankylä in Finland (68.1°N, 27.2°E) and Fairbanks International Airport in Alaska (64.5°N, 147.5°W). Daily average temperatures were below 0 °C from the middle of October to the end of March at both sites and were lowest from December to January at Sodankylä and from January to February at Fairbanks. Daily average temperatures at other sampling sites are provided in Figures S1 and S2 in the supporting information. At these sites, temperatures were below 0 °C during most of the snow accumulation period, although they occasionally exceeded 0 °C at some sites. In Yakutsk (62.0°N, 129.7°E, 97 m above sea level (asl)) in South Siberia, the average surface temperature was below 0 °C from October to the end of April (Figure S2). The temperatures near the snow sampling sites in Greenland were also below 0 °C in May of 2015 and 2016, when the snow samplings were made.

Previous studies have reported that surface snowmelt caused enhancements of C_{MBC} near the surface by a factor of 3–20 (Forsström et al., 2013; Meinander et al., 2013). It is very likely that the snowpack used for the present study underwent little melting because the surface temperatures near the sampling sites were below 0 °C during most of the snow accumulation period. In addition, visual observations of snow stratigraphy in Alaska, Greenland, and Ny-Ålesund showed no indication of snowmelt. C_{MBC} values in surface snow were low and agreed (within a factor of 2) with C_{MBC} in subsurface snow and columns of snowpack from Alaska and Greenland (see Text S1 and Figure S3 in the supporting information for more detail).

3.2. Precipitation and SWE

Continuous measurements of daily precipitation at each AWS were made with a wind-shielded weighing gauge in an open area near the station chosen to minimize wind effects and drift (Leeper et al., 2015; Taskinen & Söderholm, 2016), although wind-induced undercatch, wetting loss, and evaporation loss may still have introduced uncertainties in the measurements. For example, daily precipitation was reported to be underestimated in the Norwegian Arctic during strong wind conditions (Førland & Hanssen-Bauer, 2000).

Median values of daily precipitation (rain and snow) from October to March at Sodankylä and Fairbanks (Figures 4c and 4d) were 1.4 and 0.76 mm, respectively. We calculated cumulative SWEs at Sodankylä and Fairbanks by summing the daily amounts of precipitation up to the sampling day. We derived cumulative SWEs at five AWSs in Finland and three in Alaska, at Barrow (71.3°N, 156.8°W), Fairbanks, and Anchorage International Airport (61.2°N, 150.0°W).

Cumulative SWE estimated from AWS data correlated well with directly measured data at snow sampling sites in both Finland and Alaska (Figure S4a). A similar correlation for the snow depths is also shown in Figure S4b. For sampling sites in Finland, the cumulative SWE and snow depth values at AWSs were within about 10% of directly measured data from snowpack samples. The cumulative SWE and snow depth at AWSs in Alaska also correlated well with the direct measurements (SWE, $r^2 = 0.80$; snow depth, $r^2 = 0.65$), although both AWS data sets were underestimated by about 25%. These comparisons indicate that the overall uncertainty of the SWE values derived in this study is about 25%, which (on the basis of equation 2) leads to an uncertainty of 30% in estimations of DEP_{MBC} .

4. BC and Ionic Species in Arctic Snowpack

To characterize the deposition of BC and ionic species in snowpack in each of the six regions studied here, we used the global (Northern Hemisphere) horizontal distribution of C_{MBC} (Figure 1a) and detailed maps showing the horizontal distributions of C_{MBC} in snowpack (our data) and EF_{BC} for the five regions of the Arctic (Figure 5), together with topography. The latitudinal and longitudinal variations of C_{MBC} in all regions are summarized in Figure 6.

As shown in this and subsequent sections, C_{MBC} and DEP_{MBC} in the six regions were influenced by long-range transport from lower latitudes with higher EF_{BC} and by transport of BC from more localized sources closer to the sampling sites (Figures 1a and 1b). The contributions of the latter depend on the distributions of EF_{BC} .

4.1. Finland

EF_{BC} and C_{MBC} in the 11 columns of snowpack collected in Finland in March 2013 are shown in Figure 5a and the topography is shown in Figure 5b. Details of the locations, periods of sampling, and key parameters of BC in snowpack are provided in Table S1. The concentrations and DEP of ionic species (Na^+ , $nss-SO_4^{2-}$, NO_3^- , and NH_4^+) are provided in Table S2.

4.1.1. Concentration and Deposition Amount of BC

In Finland, BC emissions from residential combustion heating make a large contribution to EF_{BC} in winter and early spring (e.g., Stohl et al., 2013). Our analyses showed a general decrease of both C_{MBC} and DEP_{MBC} with increasing latitude, generally reflecting the changes in EF_{BC} (Figures 6a and 7a). C_{MBC} was well correlated with EF_{BC} ($r^2 = 0.87$ for all data and $r^2 = 0.57$ for data north of 65°N; Figure S5). This result suggests that localized sources of BC influenced the levels of C_{MBC} and DEP_{MBC} in Finland, although their relative contributions to those from long-range transport cannot be quantified only from this analysis.

Transport patterns at the sampling sites were investigated on the basis of backward trajectories determined using the HYSPLIT model (Text S2; Huang et al., 2010). Three-day back trajectories of precipitation and non-precipitation events showed that air parcels over Sodankylä were often transported by southerly winds from lower latitudes where BC emissions are higher (Figure S6), which supports the view that regional-scale BC emissions influence observed C_{MBC} and DEP_{MBC} . That is, air masses with high BC concentrations transported to Sodankylä from the south, followed by wet deposition of BC, contributed partly to the observed latitudinal distributions of C_{MBC} and DEP_{MBC} . Three-dimensional modeling of transport and deposition processes is needed to better quantify our interpretation of the observed C_{MBC} and DEP_{MBC} in Finland.

4.1.2. Ionic Species

Ionic species $C_{nss-SO_4^{2-}}$ (Figure 7a; $C_{NO_3^-}$ and $C_{NH_4^+}$, not shown) and their DEP values tended to decrease with increasing latitude, similarly to the decrease of C_{MBC} . $C_{nss-SO_4^{2-}}$ and $C_{NO_3^-}$ correlated strongly with C_{MBC} ($r^2 = 0.86$ and 0.77 , respectively; Figure 8a). $DEP_{nss-SO_4^{2-}}$ and $DEP_{NO_3^-}$ also correlated strongly with DEP_{MBC} ($r^2 = 0.80$ and 0.58 , respectively; Figure 8b). C_{Na^+} increased with increasing latitude north of 67°N (Figure 7a) and correlated negatively with C_{MBC} ($r^2 = 0.44$), indicating a strong influx of clean Arctic Ocean air from higher latitudes. These results show that the latitudinal distributions of BC, $nss-SO_4^{2-}$, NO_3^- , and

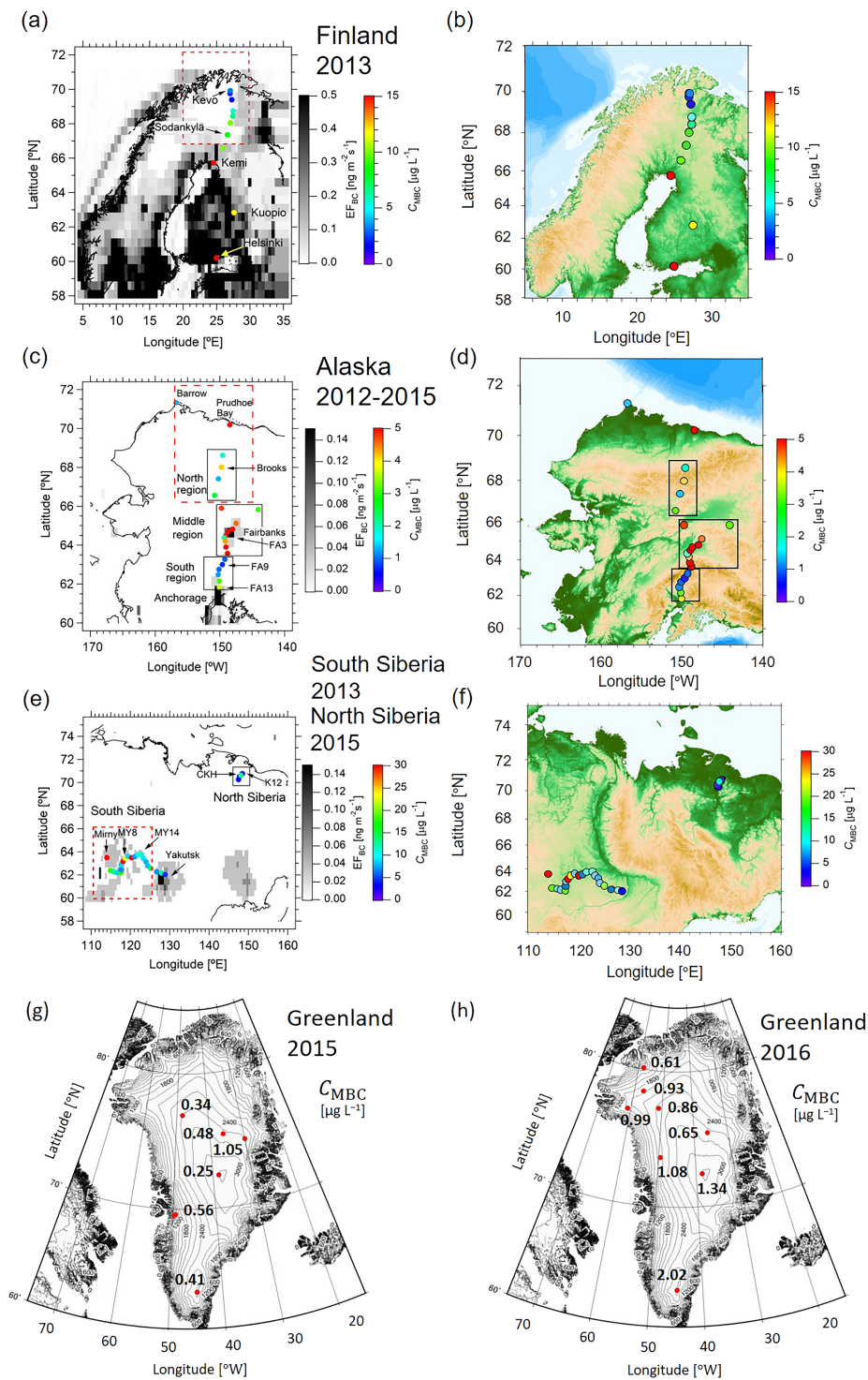


Figure 5. Maps showing (a) snowpack sampling sites in Finland in 2013 and their column-averaged BC mass concentrations (C_{MBC}) during the snow accumulation period, overlain on the distributions of the 2013 annual average anthropogenic BC emission flux (EF_{BC} ; horizontal resolution, 0.5° lat/long). (c) Same as (a) but for Alaska during 2012–2015. (e) Same as (a) but for columns of snowpack in South Siberia during the snow accumulation period of 2013 and for surface snow in North Siberia in April 2015. The red dashed rectangles in (a)–(e) mark the regions least influenced by localized BC emissions in Finland (67° – 72°N , 20° – 30°E); Alaska (66° – 72°N , 145° – 157°W), except Prudhoe Bay (70.2°N , 148.5°W); and in South Siberia (60° – 66°N , 110° – 125°E). In (c), the areas we defined as South (61.8° – 63.3°N), Middle (63.6° – 66.0°N), and North (66.6° – 68.6°N) Alaska are marked by black rectangles. (b, d, and f) Same as (a), (c), and (e) but overlain on topography (m asl). The color-coded terrain height (b) 1,000 m asl near the top of the mountains of Norway (62°N , 8°E), (d) 2,000 m asl near the top of the mountains surrounding Anchorage (61°N , 148°W), and (f) 2,000 m asl near the top of the mountains 500 km northeast of Yakutsk (62°N , 130°E). (g and h) Topographic maps of Greenland showing snow sampling sites (red dots) in 2015 and 2016, respectively. Numbers annotated at sampling sites indicate C_{MBC} in surface snow.

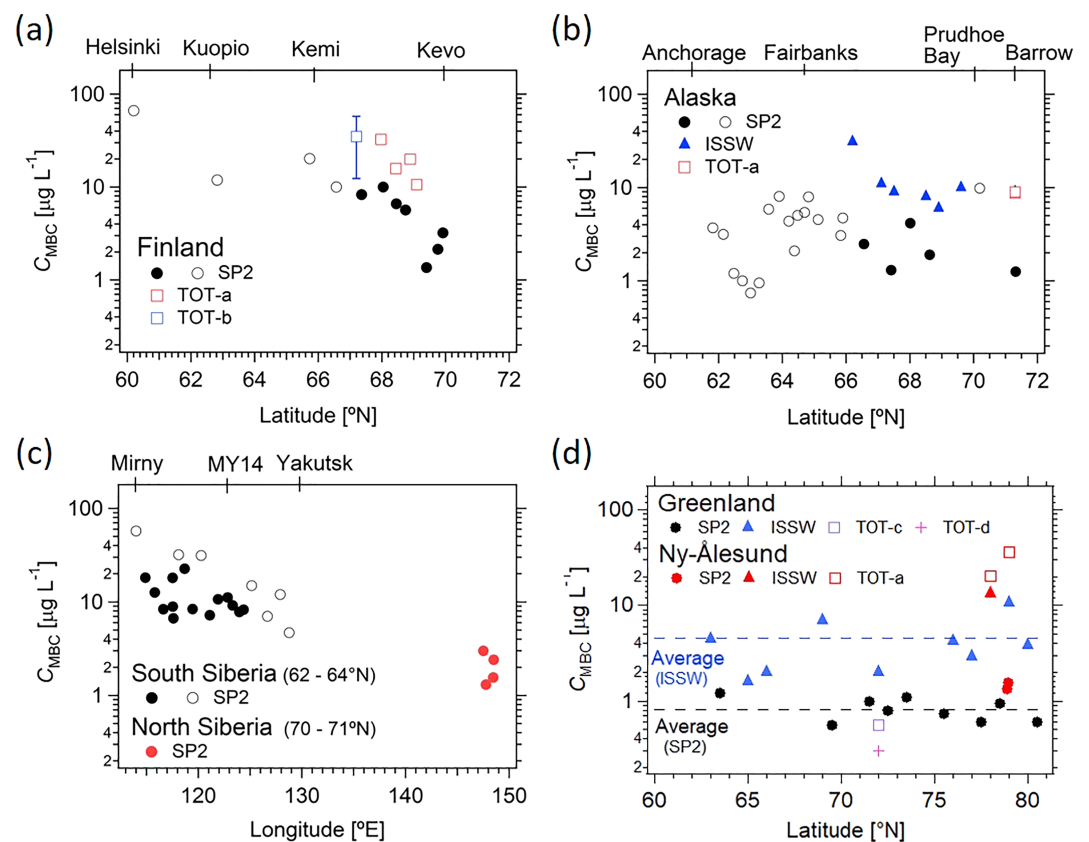


Figure 6. Latitudinal variations of C_{MBC} in snow sampled in (a) Finland, (b) Alaska, and (d) Greenland and Ny-Ålesund. (c) Longitudinal variation of C_{MBC} in snow sampled in South and North Siberia. Circles represent SP2 data derived in this study; closed circles indicate samples for which C_{MBC} was least influenced by local BC emissions, and open circles indicate samples outside this area. The area represented by closed circles corresponds to the red dashed rectangles shown in Figure 5. C_{MBC} values measured by the TOT and ISSW techniques are also shown. In (d) average C_{MBC} measured by SP2 (black) and ISSW (blue) are also shown for Greenland samples. The error bar in (a) indicates $\pm 1\sigma$ at Sodankylä. TOT-a, TOT-b, TOT-c, and TOT-d indicate measurements made at the Norwegian Polar Institute, Finnish Meteorological Institute, Georgia Institute of Technology (USA), and Snow Research Centre of the French National Centre for Meteorological Research, respectively. These previous C_{MBC} data used in this study are least influenced by the snowmelt, except for the C_{MBC} (TOT) data at Sodankylä in Finland.

Na^+ are strongly influenced by transport of anthropogenically influenced air from the south and clean air from the north.

4.1.3. BC Size Distribution

The mass and number size distributions of BC in snowpack sampled in Finland are shown in Figure 9. The BC size distributions showed low spatial variabilities and the average ($\pm 1\sigma$) f_{600} was 0.32 ± 0.07 (Figure 7a).

4.2. Alaska

Snow sampling locations, EF_{BC} , C_{MBC} , and topography are shown in Figures 5c and 5d and details of the locations and sampling dates are described in Table S3. Average concentrations, DEP, and size distributions of BC in columns of snowpack are summarized in Table S4. Data for BC in surface and subsurface snow samples are summarized in Tables S5 and S6, respectively. Concentrations and DEP of ionic species are summarized in Table S7.

4.2.1. BC Concentrations

The distribution of EF_{BC} in Alaska is highly irregular; it is high in populated areas (Fairbanks and Anchorage) and very low in other areas (Figures 5 and 7b). To interpret the horizontal distribution of C_{MBC} , we classified the Alaskan sampling locations into five regions on the basis of the distribution of

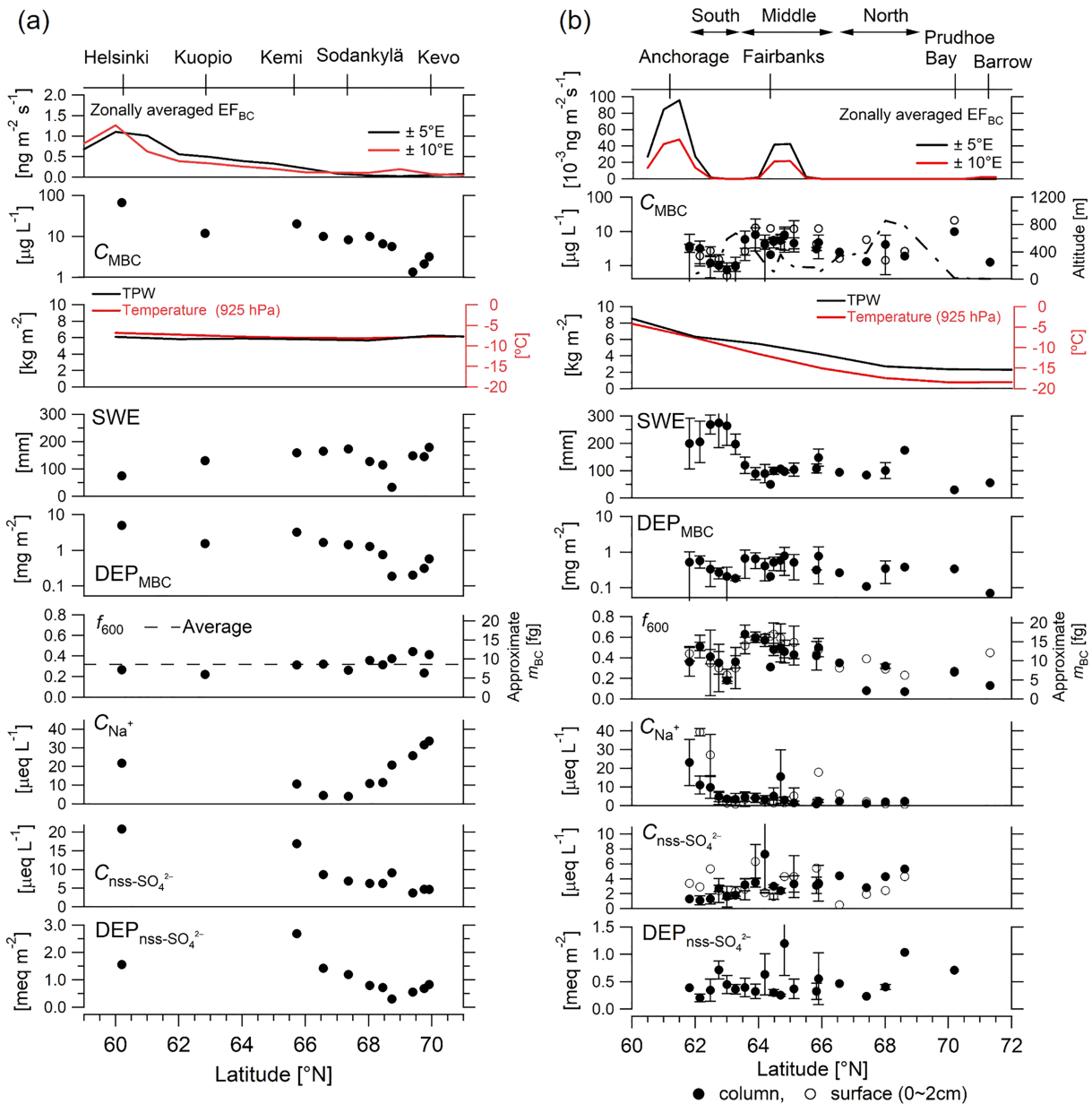


Figure 7. (a) Finland data from winter 2012 to spring 2013. Top and third panels: zonally averaged anthropogenic BC emission flux (EF_{BC} ; horizontal resolutions of $1^\circ\text{ lat} \times 10^\circ\text{ long}$ [black line] and $1^\circ\text{ lat} \times 20^\circ\text{ long}$ [red line]) and latitudinal variations of seasonally averaged total precipitable water (TPW; horizontal resolution of 2°N for longitudes $24^\circ\text{--}26^\circ\text{E}$) from winter 2012 to spring 2013, calculated from temperature and RH (Bolton, 1980; Murphy & Koop, 2005) obtained from NCEP/NCAR global reanalysis data (horizontal resolution of $2.5^\circ\text{ lat/long}$), together with the average temperature at 925 hPa for the same period. Other panels: latitudinal variations of C_{MBC} , SWE, DEP_{MBC} , f_{600} (approximate m_{BC}), C_{Na^+} , $C_{nss-SO_4^{2-}}$, and $DEP_{nss-SO_4^{2-}}$ in snow. Dashed line indicates regionally averaged f_{600} . Approximate m_{BC} is derived from the f_{600} – m_{BC} correlation in Figure A1. (b) Same as (a) but for data from Alaska during 2012–2015 for longitudes $149^\circ\text{--}151^\circ\text{W}$. Error bars indicate $\pm 1\sigma$. The dash-dot line in the panel showing the C_{MBC} distribution indicates altitude. Column-averaged values of C_{Na^+} (181 $\mu\text{eq/L}$) and $C_{nss-SO_4^{2-}}$ (20.7 $\mu\text{eq/L}$) in snowpack and surface snow values of C_{Na^+} (371 $\mu\text{eq/L}$) and $C_{nss-SO_4^{2-}}$ (43.3 $\mu\text{eq/L}$) in samples from Prudhoe Bay are not shown.

EF_{BC} (Figure 5c): South region ($61.8^\circ\text{--}63.3^\circ\text{N}$), Middle region ($63.5^\circ\text{--}66.0^\circ\text{N}$), North region ($66.5^\circ\text{--}68.7^\circ\text{N}$), Prudhoe Bay (location PB, 70.2°N ; see tables in the supporting information for details of this sample location and others mentioned below), and Barrow (location BA, 71.3°N). High values of C_{MBC} near Anchorage and Fairbanks appear to be associated with locally high EF_{BC} (Figure 5c).

Table S8 provides regionally averaged BC parameters derived from columns of snowpack for the five regions of Alaska. Figure 7b shows the latitudinal distributions of column-averaged C_{MBC} , SWE, DEP_{MBC} , f_{600} (m_{BC}), C_{Na^+} , $C_{nss-SO_4^{2-}}$, $DEP_{nss-SO_4^{2-}}$, and those in surface snow samples during 2012–2015, together with zonally

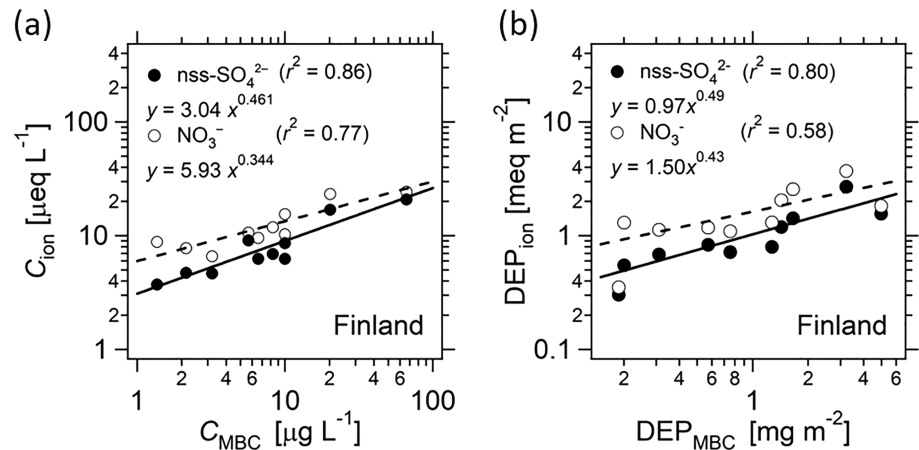


Figure 8. (a) Correlation between ionic species (nss-SO_4^{2-} and NO_3^-) concentrations (C_{ion}) and BC mass concentrations (C_{MBC}) in columns of snowpack from Finland. (b) Same as (a) but for the deposition amounts of these (DEP_{ion} and DEP_{MBC}) in snowpack from Finland. The solid and dashed lines indicate the least squares fitted regressions for nss-SO_4^{2-} and NO_3^- , respectively.

averaged EF_{BC} . The latitudinal variation of column-averaged C_{MBC} was generally similar to those of C_{MBC} in surface and subsurface snow samples. The characteristics of C_{MBC} for each region are summarized as below.

4.2.1.1. South Region

C_{MBC} in the South region was low, except near Anchorage, and C_{Na}^+ and SWE were generally high (Figure 7b). Three-day back trajectories from Anchorage indicated frequent flows of maritime air parcels

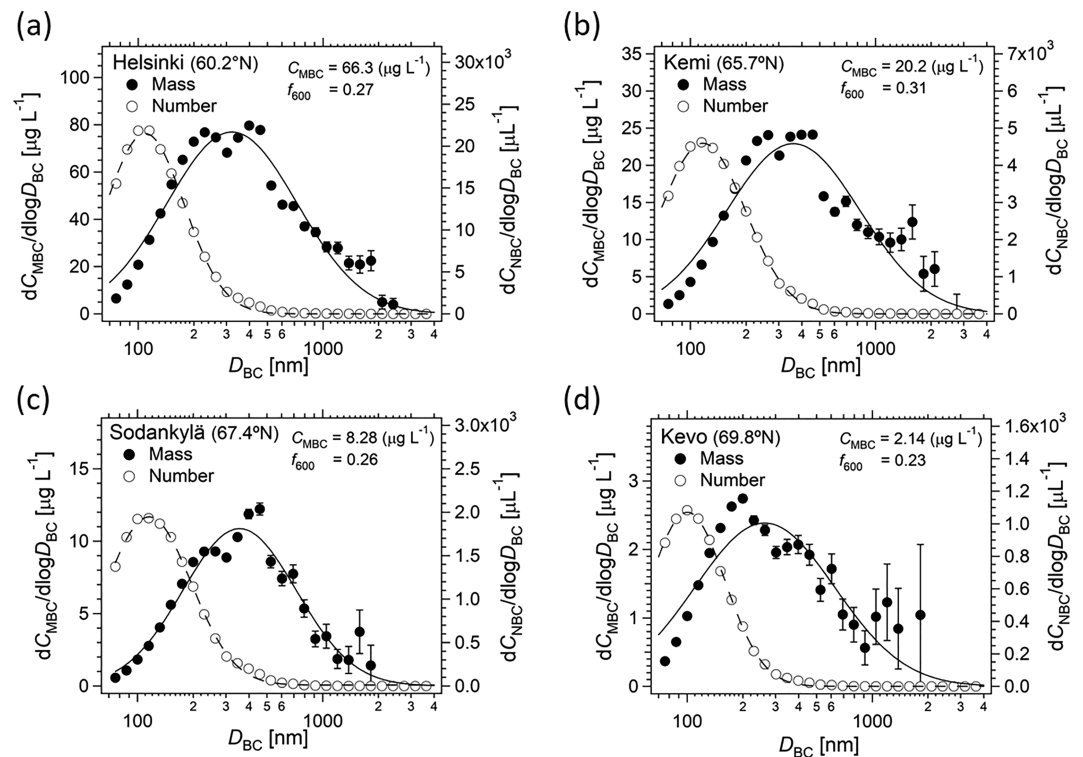


Figure 9. BC mass and number size distributions in columns of snowpack from near (a) Helsinki, (b) Kemi, (c) Sodankylä, and (d) Kevo in Finland. The solid and dashed lines indicate lognormal fitted BC mass and number size distributions, respectively. Error bars indicate $\pm 1\sigma$ of a Poisson distribution. C_{MBC} and f_{600} are annotated at the top right of each panel. MMD, CMD, σ_{gm} , σ_{gc} , f_{600} , and m_{BC} are summarized in Table S1.

into the South region (Figures S7a and S7b). It is likely that significant fractions of BC particles had already been removed by precipitation during transport before these air parcels reached the South region. Because of the low C_{MBC} , DEP_{MBC} was moderate, despite the high SWE.

4.2.1.2. Middle Region

Average C_{MBC} in the Middle region ($5.11 \pm 1.87 \mu\text{g/L}$) was higher by a factor of about 2 than in the North region ($2.46 \pm 1.22 \mu\text{g/L}$) and higher by a factor of about 3 than in the South region ($1.79 \pm 1.29 \mu\text{g/L}$), shown in Table S8. These differences correspond to higher EF_{BC} in the Middle region, which is surrounded by mountains (Figures 5d and 7b) and where temperature inversions are common occurrences (Figure A2). PBL height was very low in Fairbanks (~ 400 m) due to strong cooling at the surface (Figure A3). Accumulation of high concentrations of aerosols, including BC from anthropogenic sources, has been reported in the PBL over Fairbanks (Tran & Mölders, 2011; Ward et al., 2012).

4.2.1.3. North Region

The North region is relatively free of localized BC emissions. Therefore, observed C_{MBC} data in this region can be used as a benchmark for these latitudes in Alaska and for comparison with the other regions (section 5).

4.2.1.4. Prudhoe Bay

C_{MBC} at Prudhoe Bay was the highest in samples from Alaska (Figure 7b). Aircraft measurements near Prudhoe Bay have shown high ambient BC mass concentrations due to emissions associated with gas flaring from commercial oil and gas production (Brock et al., 2011), although the present EF_{BC} does not include these emissions. $C_{\text{nss-SO}_4^{2-}}$ in both snowpack and surface snow at Prudhoe Bay were also the highest values in Alaska (20.7 and 43.3 $\mu\text{eq/L}$, respectively), reflecting high emissions of SO_2 and nss-SO_4^{2-} from petroleum fields. These data give a clear indication that BC particles from flaring of petroleum gas strongly influence C_{MBC} in surrounding areas.

4.2.1.5. Barrow

C_{MBC} and DEP_{MBC} were very low at Barrow. Three-day back trajectories from Barrow (Figures S7c and S7d) show that mainly clean air parcels from the Arctic Ocean were transported to Barrow on both precipitation and nonprecipitation days. However, the data for Barrow were obtained only during 2013 and no other samples were collected nearby, so the Barrow data may not be representative of this latitude in Alaska.

4.2.2. Correlation of BC With Ionic Species

Column-averaged $C_{\text{nss-SO}_4^{2-}}$ was low in the South region, but it was more or less uniform in the other two regions (Figure 7b). $C_{\text{nss-SO}_4^{2-}}$ and $C_{\text{NO}_3^-}$ were not correlated with C_{MBC} if the data from near Fairbanks and Anchorage (not shown) were excluded. Similarly, $\text{DEP}_{\text{nss-SO}_4^{2-}}$ and $\text{DEP}_{\text{NO}_3^-}$ were not correlated with DEP_{MBC} . The lack of correlation between BC and ionic species suggests that their sources were not co-located. More detailed discussion is provided in sections 4.2.4 and 5.1.

4.2.3. Size Distribution of BC

Figure 10 shows normalized mass and number size distributions of BC in columns of snowpack from six locations in Alaska that span from low latitudes (location FA13 near Anchorage) to high latitudes (location BA, Barrow) for each sampling year. Table S8 summarizes important parameters of BC size distributions for each of the five regions we considered in Alaska.

Bimodal mass size distributions were observed near Anchorage (location FA13) and Fairbanks (location FA3), but the mass size distribution between these two locations was monomodal and f_{600} was correspondingly low. At locations north of Brooks, the size distributions were almost monomodal, and f_{600} decreased monotonically with increasing latitude (Figure 7b). Bimodal distributions were observed only in the vicinity of large sources of anthropogenic BC (Anchorage and Fairbanks).

Aircraft measurements in Asia have shown that larger BC particles are selectively removed by precipitation owing to their higher activities as cloud condensation nuclei (Kondo et al., 2016; Moteki et al., 2012). Simultaneous measurements of BC size distributions in ambient air and rainwater in Tokyo have shown that the activity of relatively fresh BC particles as cloud condensation nuclei was higher for larger BC particles (Ohata et al., 2016). In Anchorage and near Fairbanks, wood burning for winter heating is an important source of BC (Wang & Hopke, 2014; Ward et al., 2012). The size distributions of BC from wood burning generally show a shift to larger sizes, compared to those from anthropogenic sources (Bond et al., 2013; Schwarz et al., 2008), although the measurements were limited to diameters less than about 700 nm.

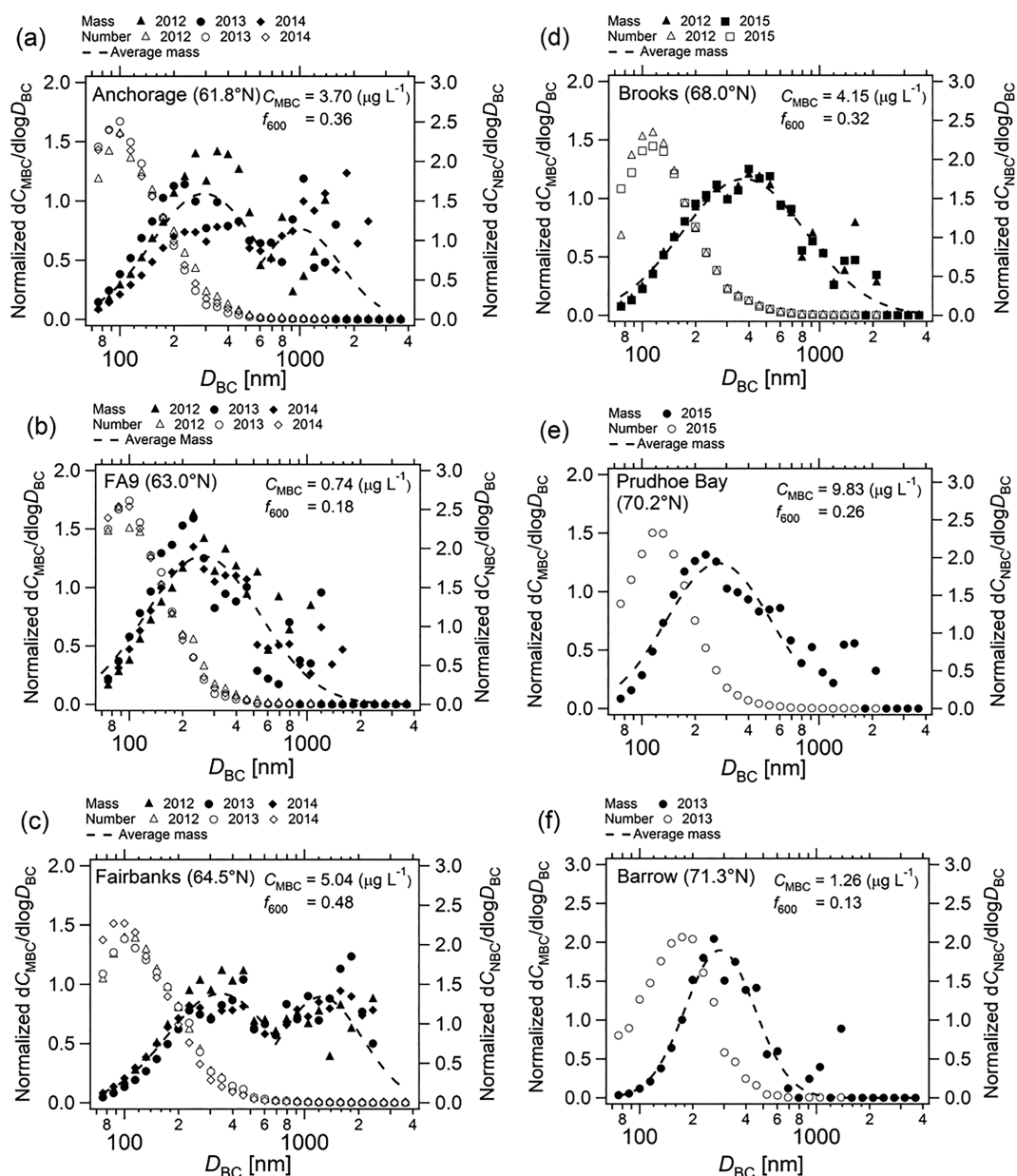


Figure 10. Mass and number size distributions of BC normalized by total BC mass and number concentrations, respectively, in snowpack in Alaska. (a) Near Anchorage in the South region, (b) FA9 located between Anchorage and Fairbanks (South region), (c) near Fairbanks in the Middle region, (d) Brooks (North region), (e) Prudhoe Bay, and (f) Barrow. The dashed lines are lognormal fitted BC mass size distributions for the average BC size distributions. Average C_{MBC} and f_{600} are annotated at the top right of each panel.

In addition, the efficiency of below-cloud scavenging of aerosols by falling snow also increases with increasing aerosol size above 200 nm (Murakami et al., 1985; Zhang et al., 2013), although this effect would likely be less important than nucleation scavenging (Moteki et al., 2019; Ohata et al., 2016). These processes in total may amplify BC mass concentrations at diameters larger than about 1 μm in falling snow in these areas.

Values of f_{600} decreased northward from 65°N (Figure 7b). The size distributions of ambient BC have been observed to shift to smaller diameters during transport from sources because of the selective removal of larger particles, as discussed above. The decrease with increasing latitude of f_{600} of BC in snowpack that we observed distant from anthropogenic sources suggests a corresponding decrease of f_{600} of BC in ambient air.

At Prudhoe Bay, a monomodal BC mass size distribution ($f_{600} = 0.26$; Figure 10e) was observed in snowpack, in contrast with the size distributions in samples from Fairbanks and near Anchorage, which suggests that f_{600} values of BC emitted by gas flaring are likely to be smaller than those of BC particles emitted from urban sources, including wood burning.

4.2.4. Latitudinal Similarities and Differences of Key Parameters in Finland and Alaska

Because of the similarity of the latitudinal ranges of sampling locations in Finland and Alaska, we compared key BC and ionic species parameters in the two regions (Figure 7) to characterize their features and better understand processes in controlling the deposition of BC and ions.

In Finland, zonally averaged EF_{BC} decreased gradually with increasing latitude, except for highly localized sources near Helsinki and Kuopio (Figures 5a and 7a). In contrast, EF_{BC} in Alaska was locally high around Fairbanks and Anchorage and close to zero in other areas (Figures 5c and 7b). Despite these differences in the latitudinal distributions of EF_{BC} , C_{MBC} decreased gradually with increasing latitude north of $63.5^{\circ}N$ in both Finland and Alaska, except for Prudhoe Bay ($70.2^{\circ}N$). Thus, it appears that the contributions of localized BC emissions to C_{MBC} at these latitudes were relatively small and that C_{MBC} was strongly influenced by meridional transport of BC emitted from wider regions at lower latitudes.

In Finland, SWE increased with increasing latitude, except near the sampling site at $68.7^{\circ}N$ (Figure 7a), whereas in Alaska, SWE showed a large decrease north of about $63^{\circ}N$ and continued to decrease with increasing latitude (Figure 7b). Seasonally averaged water vapor mixing ratio (w) and total precipitable water (TPW) calculated from temperature and RH showed only small latitudinal variations in Finland (Figures 7a and S8c), associated with a similar temperature variation at 925 hPa. In contrast, TPW and w in Alaska decreased with increasing latitude associated with a corresponding temperature decrease (Figures 7b and S8g). The patterns of latitudinal variations of temperature and w were similar for other pressures (700–1,000 hPa; Figure S8).

The differences of the latitudinal variations of SWE for both Finland and Alaska correspond well to those of w and TPW. In both regions, the latitudinal variations of w and TPW were mainly controlled by corresponding variations of temperature, which regulates the saturation water vapor mixing ratio. The correlation between SWE and TPW is discussed in section 5.1, together with the data from other regions.

DEP_{MBC} generally decreased with increasing latitude in both Finland and Alaska (north of $63.5^{\circ}N$; Figure 7), mainly in response to latitudinal variations of C_{MBC} .

Values of f_{600} were relatively uniform in Finland, whereas they decreased gradually with increasing latitude in Alaska north of $63.5^{\circ}N$ (Figure 7). It is likely that BC in Alaska was influenced more by sources at far greater distances from the sampling sites (as mentioned earlier in this section in our discussion of EF_{BC}). The influence of distant sources is discussed in more detail in section 5.1.

C_{Na}^{+} increased with increasing latitude in northern Finland (north of $67^{\circ}N$), whereas it was high in southern Alaska (south of $63^{\circ}N$). C_{Na}^{+} in both areas was influenced by transport of clean maritime air parcels, with similar values of SWE in these areas (Figure 7). $C_{nss-SO_4}^{2-}$ and $DEP_{nss-SO_4}^{2-}$ decreased with increasing latitude in Finland, similarly to the latitudinal changes in C_{MBC} and DEP_{MBC} .

In contrast, $C_{nss-SO_4}^{2-}$ and $DEP_{nss-SO_4}^{2-}$ in northern Alaska were more uniform (Figure 7b), although the distribution of emission flux of anthropogenic SO_2 in Alaska is highly irregular (Tran et al., 2011; Yang et al., 2018). Differences in the distributions of emission flexes of BC (Figure 1b) and SO_2 , combined with the formation processes of sulfate during transport (Yang et al., 2018) may contribute to this small latitudinal variation.

4.3. Siberia

Snow sampling locations, EF_{BC} , C_{MBC} , and topography in Siberia are shown in Figures 5e and 5f. Table S9 summarizes the locations and dates of sampling of snowpack and the values of key parameters. Table S10 summarizes the concentrations and DEP of ionic species in the columns of snowpack from South Siberia.

4.3.1. South Siberia

The longitudinal distributions of EF_{BC} , C_{MBC} , SWE, TPW, DEP_{MBC} , f_{600} (m_{BC}), $C_{nss-SO_4}^{2-}$, $DEP_{nss-SO_4}^{2-}$, and altitude of sampling in South Siberia are shown in Figure 11.

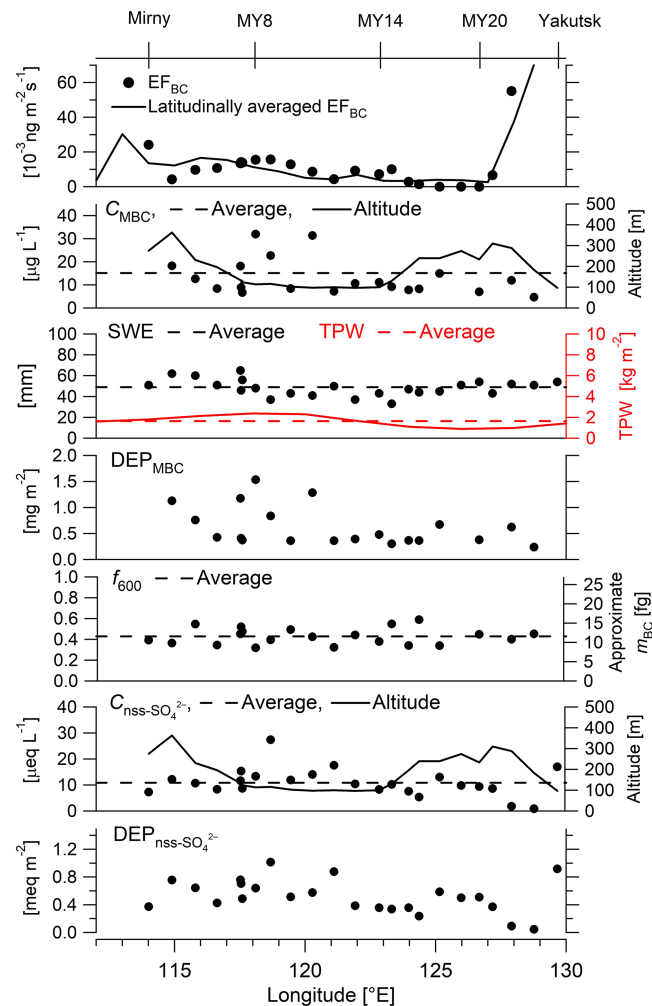


Figure 11. Longitudinal distributions in South Siberia of (top panel) EF_{BC} (horizontal resolution 1.0° lat/long) and average EF_{BC} for latitude 60° – 66° N (solid line) and (second panel to bottom panel) altitude, C_{MBC} in snowpack columns, SWE, average TPW from winter 2012 to spring 2013 (horizontal resolution of 2° E for longitudes and averaged for a latitude range of 62° – 64° N), DEP_{MBC} , f_{600} , $C_{nss-SO_4^{2-}}$, and $DEP_{nss-SO_4^{2-}}$. Regionally averaged C_{MBC} , SWE, TPW, f_{600} , and $C_{nss-SO_4^{2-}}$ are shown as dashed lines. Values of EF_{BC} of $160 \times 10^{-3} \text{ ng m}^{-2} \text{ s}^{-1}$ near Yakutsk, and C_{MBC} of $57.5 \text{ } \mu\text{g/L}$ and DEP_{MBC} of 2.93 mg/m^2 at Mirny are not shown.

C_{MBC} and $C_{nss-SO_4^{2-}}$ in South Siberia were systematically higher than in Alaska likely because the South Siberian sampling sites are generally closer to BC sources than those in Alaska. Moreover, many of the sampling locations in South Siberia are surrounded by mountains, especially to the east of the sampling region (Figure 5f). Because the average PBL height in South Siberia (Yakutsk) is only about 500 m, BC emitted there can accumulate within it (Figure A3). The lowest altitude within the sampled area is between longitudes 117° and 121° E, where C_{MBC} and $C_{nss-SO_4^{2-}}$ at individual sample locations were higher than their averages. Low PBL height can enhance aerosol concentrations in the PBL. This interpretation of our data is supported by three-day back trajectories from December 2012 to March 2013, which show that most of the air parcels reaching South Siberia remained over Russia during that period (Figures S9a and S9b) with the zonal component of the trajectories dominantly from the west, reflecting the topography. These transport processes may have weakened the correlation between C_{MBC} and EF_{BC} . In contrast, the longitudinal variability of SWE in South Siberia was less than 16%, somewhat smaller than that of TPW (31%; $1.64 \pm 0.51 \text{ kg/m}^2$), indicating that topography had little influence on the spatial distribution of precipitation there.

$C_{nss-SO_4^{2-}}$ and $C_{NO_3^-}$ were poorly correlated with C_{MBC} ($r^2 = 0.03$ and 0.07 , respectively; not shown), although these concentrations were generally high between longitudes 117° and 121° E. The poor correlation may be due to inhomogeneous and uncorrelated distributions of emission fluxes of BC, SO_2 , and NO_x in

regions, which could have influenced the concentrations of the aerosols over the sampling region as a result of transport and formation of sulfate and nitrate.

4.3.2. North Siberia

No snowpack columns were collected in North Siberia for this study. The median values of C_{MBC} and C_{NBC} in snow samples collected in April 2015 were lower by factors of 4.4 and 3.0, respectively, than those in columns of snowpack from South Siberia, except at location CKH (70.6°N, 148.1°E; Figure 5e and Table 4). These lower values are consistent with the much lower EF_{BC} in North Siberia than in South Siberia (Figure 5e). Moreover, the area of sampling in North Siberia is not surrounded by mountains (Figure 5f), thus reducing the accumulation of locally emitted BC. Back trajectories from 1 to 15 April 2015 (day of sampling) show that many of the air parcels that reached location K12 (70.8°N, 148.5°E) via the Arctic Ocean had consistently high RH (Figure S9c). These transport pathways possibly resulted in low ambient BC concentrations, which in turn lowered C_{MBC} . The high C_{MBC} at site CKH (Figure 5e) also suggests that C_{MBC} can be influenced by local BC emissions that are not represented in the regional EF_{BC} data for this area.

4.3.3. BC Size Distributions in South and North Siberia

The median value of f_{600} in snowpack in South Siberia was high (0.43) with low variability (~19%; Figure 11 and Table 4). The BC mass and number size distributions in snowpack (bimodal distributions) at location MY-8 (Figure 12a) are typical of the South Siberian samples and are similar to those from the Middle region of Alaska. The high f_{600} values in South Siberia confirm that BC in the region was strongly influenced by emissions on a regional scale. In addition, low precipitation (represented by low SWE, shown in Figure 11 and Table 4) in South Siberia suggests low efficiency of wet removal of BC, thus reducing the effect of size-selective removal of larger BC particles.

The median values of MMD and f_{600} in North Siberia were 252 nm and 0.29, respectively (Table 4). The monomodal size distributions at location K12 (Figure 12b) are typical of surface snow sampled in North Siberia and are considerably lower than in South Siberia, likely because of the greater aging of air parcels that reached North Siberia.

4.4. Greenland

We collected surface and subsurface snow samples at 22 locations in Greenland (including 12 AWSs) during 2012–2016 (Figures 1a, 5g, and 5h). The concentrations and size distributions of BC in surface and subsurface snow samples are summarized in Tables S11 and S12, respectively.

Figures 5g and 5h show the distributions of C_{MBC} at sample sites in Greenland for 2015 and 2016. Much higher concentrations were observed at SIGMA site A, Qaanaaq, and Thule in 2012, 2013, and 2014 (not shown), but these data were excluded from our analyses because they were strongly influenced by local anthropogenic sources.

Figure 13 shows the latitudinal variations of altitude, C_{MBC} , and f_{600} at sites in Greenland. The mass and number size distributions of BC in surface snow at two sampling sites (Figure S10) are typical of the Greenland samples. C_{MBC} (surface snow) in Greenland was uniformly rather low, despite large differences in altitude. This phenomenon was observed also for subsurface snow samples (Figure S11). C_{MBC} , C_{NBC} , MMD (f_{600}), and CMD did not correlate with either altitude or latitude (not shown). The uniformly low C_{MBC} and C_{NBC} probably reflect horizontally uniform low BC concentrations in the lower troposphere over Greenland because the sampling sites are distant from continental sources of BC (Figure 1b).

The average values ($\pm 1\sigma$) of C_{MBC} (surface snow) over Greenland for 2015 and 2016 were 0.52 ± 0.28 and 1.06 ± 0.45 $\mu\text{g/L}$, respectively, and average C_{MBC} (surface snow) was 0.81 ± 0.46 $\mu\text{g/L}$. The average values ($\pm 1\sigma$) of MMD, CMD, f_{600} , and m_{BC} for surface snow samples were reasonably uniform at 200 ± 30 nm, 93 ± 8 nm, 0.16 ± 0.07 , and 3.8 ± 0.8 fg, respectively.

4.5. Ny-Ålesund (Spitsbergen)

We collected surface, subsurface, and column snowpack samples at two sites at Ny-Ålesund in April 2013, one site near the Baseline Surface Radiation Network (BSRN) facility (11 m asl) and the other at Austre-Brøggerbreen Glacier (300 m asl). Table S13 summarizes the snowpack column, surface snow, and subsurface snow data of BC for these sites. Table S14 summarizes those for ionic species. Figure 13 shows the altitudes of the sites, C_{MBC} , and f_{600} . C_{MBC} was similar to the average for Greenland, depended little on location,

Table 4
Results of Snow Analyses for Surface Snow and Snowpack Samples Collected in Six Regions of the Arctic During the Snow Accumulation Periods of 2012–2016, and w Near Surface (1,000 hPa) and TPW Estimated From NCEP/NCAR Global Reanalysis Data

Snowpack column samples	Region	Sampling period	C_{MBC} ($\mu\text{g/L}$)	C_{NBC} (μL)	SWE (mm)	DEP_{MBC} ($\mu\text{g/m}^2$)	DEP_{NBC} ($10^3/\text{m}^2$)	w (g/kg)	TPW (kg/m^2)	MMD (nm)	CMD (nm)	σ_{gm}	σ_{gc}	f_{600}	m_{BC} (fg)
Snowpack column samples	Finland	2013	8.28 (4.44, 10.9)	934 (548, 1307)	145 (121, 162)	1273 (442, 1597)	114 (65.8, 189)	2.16 (1.97, 2.52)	6.40 (6.31, 6.55)	358 (321, 385)	110 (106, 116)	2.25 (2.1, 2.37)	1.69 (1.64, 1.71)	0.31 (0.26, 0.37)	8.46 (7.4, 9.18)
	Alaska	2012– 2015	3.43 (1.45, 4.97)	297 (223, 428)	106 (97.1, 199)	363 (265, 556)	41.6 (29.3, 48.7)	1.03 (0.58, 1.89)	4.17 (2.55, 5.90)	321 (284, 355)	104 (95.3, 117)	1.99 (1.91, 2.07)	1.74 (1.66, 1.8)	0.39 (0.31, 0.49)	9.61 (7.84, 11.8)
	South Siberia	2013	10.7 (8.28, 18.1)	922 (698, 1332)	49 (43, 52.5)	427 (368, 839)	49.1 (30, 75.8)	0.31 (0.20, 0.44)	1.76 (1.16, 2.31)	338 (320, 359)	105 (100, 110)	1.93 (1.87, 1.96)	1.79 (1.73, 1.8)	0.43 (0.36, 0.47)	11.5 (9.97, 13.7)
	North Siberia	-	-	-	-	-	-	-	-	-	-	-	-	-	-
	Greenland	-	-	-	-	-	-	-	-	-	-	-	-	-	-
	Ny- Ålesund	2013	1.45 (1.4, 1.5)	332 (313, 350)	253 (197, 308)	355 (288, 422)	79.7 (66, 93.3)	1.64	4.33	216 (214, 217)	106 (105, 107)	1.74 (1.74, 1.75)	1.57 (1.57, 1.58)	0.13 (0.12, 0.14)	4.39 (4.3, 4.48)
	Finland	-	-	-	-	-	-	-	-	-	-	-	-	-	-
	Alaska	2012– 2015	3.71 (1.69, 7.16)	350 (240, 651)	-	-	-	-	-	314 (264, 394)	101 (94.5, 112)	2.04 (1.91, 2.21)	1.68 (1.62, 1.76)	0.44 (0.3, 0.55)	9.57 (6.86, 13.7)
	South Siberia	-	-	-	-	-	-	-	-	-	-	-	-	-	-
	North Siberia	2015	2.41 (1.56, 3.01)	311 (287, 560)	-	-	-	-	-	252 (227, 265)	107 (98.3, 109)	1.81 (1.75, 1.96)	1.66 (1.64, 1.74)	0.29 (0.25, 0.38)	6.89 (5.44, 7.76)
Surface samples	Greenland	2012– 2016	1.11 (0.6, 4.76)	307 (173, 1340)	-	-	-	-	-	200 (191, 220)	90.9 (84.3, 98.3)	1.75 (1.66, 1.9)	1.65 (1.63, 1.69)	0.14 (0.1, 0.22)	3.75 (3.44, 4.4)
	Ny- Ålesund	2013	0.97 (0.7, 1.48)	208 (132, 355)	-	-	-	-	-	229 (213, 266)	104 (103, 117)	1.75 (1.74, 1.76)	1.61 (1.59, 1.63)	0.14 (0.13, 0.14)	6.16 (5.41, 6.91)

Note. Median (25th and 75th percentiles in parentheses) values of C_{MBC} , C_{NBC} , SWE, DEP_{MBC} , DEP_{NBC} , w , TPW, MMD, and CMD are shown, as well as geometric standard deviations of mass and number size distributions (σ_{gm} and σ_{gc} , respectively), f_{600} , and m_{BC} .

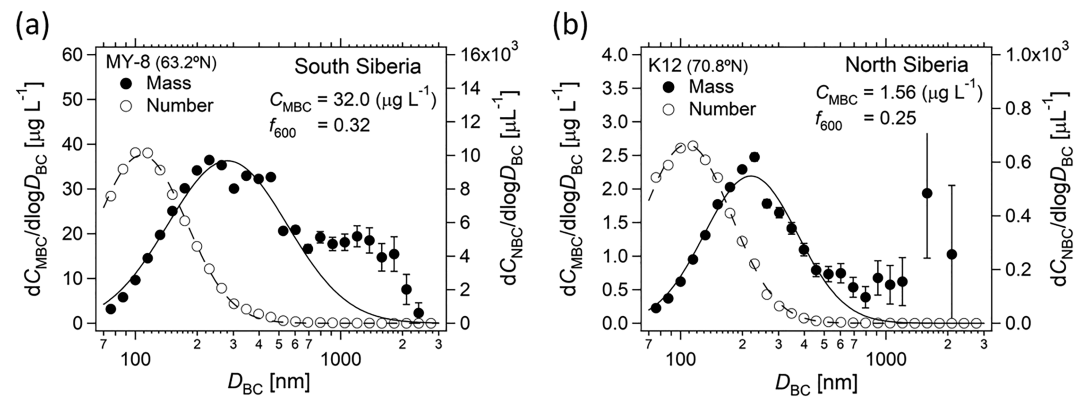


Figure 12. (a) BC mass and number size distributions in column of snowpack at site MY-8 (63.2°N, 118.1°E) in South Siberia. (b) Same as (a) but for surface snow at site K12 (70.8°N, 148.5°E) in North Siberia. C_{MBC} and f_{600} are annotated at the top right of each panel. Error bars indicate $\pm 1\sigma$ of a Poisson distribution.

and was comparable to the averages at Barrow (Alaska), Kevo (Finland), and in North Siberia. $C_{nss-SO_4^{2-}}$ at Ny-Ålesund was also comparable to that in samples from northern Alaska and Kevo. C_{MBC} (subsurface) at Ny-Ålesund was higher than the average C_{MBC} (subsurface) in Greenland by a factor of 2.4 (Figure S11).

SWE at the Glacier site was 2.6 times higher than that at the BSRN site (Table S13), so DEP_{MBC} at the Glacier site was higher by a factor of 2.2, as described in detail by Sinha et al. (2018). The size distributions (f_{600}) at the two Ny-Ålesund sites were similar to those in Greenland (Figure 13).

5. Regional Comparison of Average EF_{BC} and Other Key BC Parameters

In section 4, we characterized the spatial distributions of key BC parameters (C_{MBC} , C_{NBC} , SWE, DEP_{MBC} , DEP_{NBC} , MMD, CMD, f_{600} , and m_{BC}) in six regions of the Arctic. The median values of these parameters for each region are summarized in Table 4 and the C_{MBC} values are summarized in Figure 6.

To compare these distributions to regional distributions of EF_{BC} , we first identified the areas in and around each of the six sampling regions where EF_{BC} (horizontal resolution, 0.5° lat/long) was less than 0.1 ng m⁻² s⁻¹. We considered these areas to be the areas where C_{MBC} was least influenced by local BC emissions. This selection was made for northern Finland (67°–72°N, 20°–30°E), northern Alaska (66°–72°N, 145°–157°W), except for Prudhoe Bay, and South Siberia (60°–66°N, 110°–125°E). The selected areas are indicated in Figures 5a (northern Finland), 5c (northern Alaska), and 5e (South Siberia). For this analysis, we used the data from within these areas. For the other areas, the ranges of the selected areas of EF_{BC} and the snow sampling regions were almost the same (Figure 1a). The selected C_{MBC} data used for the following analyses are shown in Figure 6 as closed circles.

5.1. BC, $nss-SO_4^{2-}$, and SWE

Regionally averaged C_{MBC} selected on the basis of areas of low EF_{BC} were very low in the areas where EF_{BC} was close to zero (Alaska, North Siberia, Greenland, and Ny-Ålesund), whereas in South Siberia and Finland, they were larger than in Alaska by factors of 5.1 and 2.7, respectively (Figure 14). Regionally averaged $C_{nss-SO_4^{2-}}$ in South Siberia and Finland were also higher than in Alaska by factors of 2.7 and 1.5, respectively.

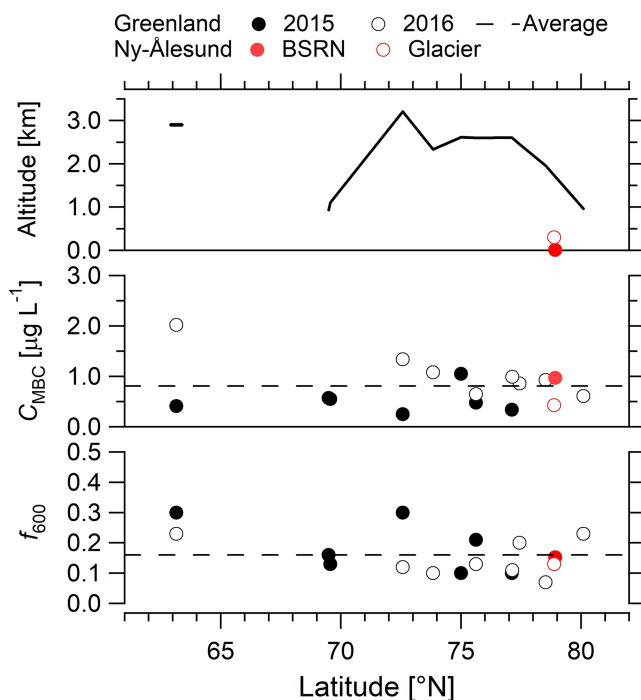


Figure 13. Latitudinal variations of altitude, C_{MBC} in surface snow, and f_{600} for samples collected in Greenland in 2015 and 2016 and at Ny-Ålesund near the Baseline Surface Radiation Network (BSRN) facility and Austre-Brøggerbreen Glacier in 2013. Dashed lines indicate regionally averaged C_{MBC} (0.81 μg/L) and f_{600} (0.16) for the Greenland samples.

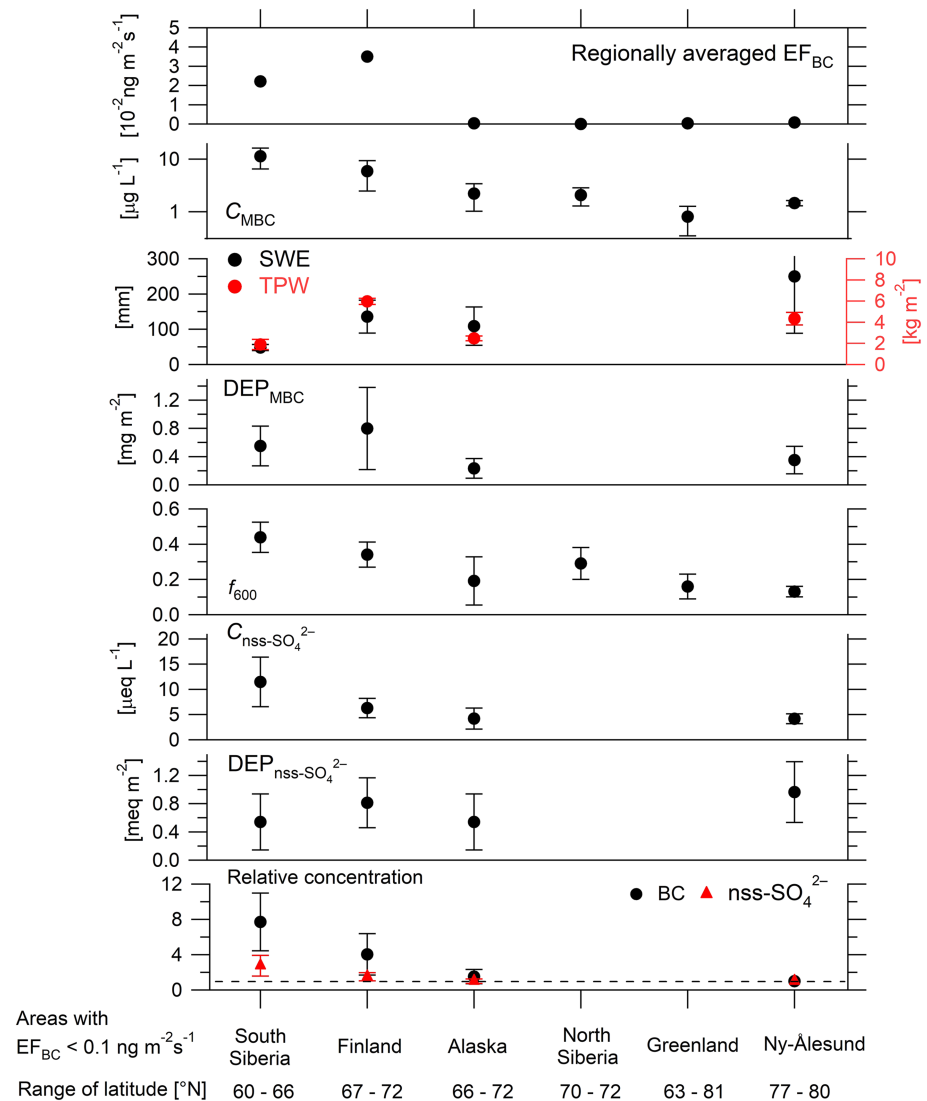


Figure 14. Regionally averaged EF_{BC} , C_{MBC} , SWE, TPW, DEP_{MBC} , f_{600} , $C_{nss-SO_4^{2-}}$, $DEP_{nss-SO_4^{2-}}$, and the ratios of C_{MBC} and $C_{nss-SO_4^{2-}}$ to those at Ny-Ålesund, in the areas least influenced by local BC emissions. Latitude ranges of areas of $EF_{BC} < 0.1 \text{ ng m}^{-2} \text{ s}^{-1}$, which include the selected sampling areas, are also shown. Error bars represent $\pm 1\sigma$.

Clearly, these differences can be attributed to higher emissions of BC and SO_2 in South Siberia and Finland, owing to the low PBL heights in those regions (Figure A3), and, in part, the favorable topography in those regions for accumulation of anthropogenic aerosols.

The ratios of the regionally averaged C_{MBC} in South Siberia and Finland to that at Ny-Ålesund were 7.7 and 4.0, respectively (Figure 14). The corresponding ratios for $C_{nss-SO_4^{2-}}$ were 2.8 and 1.5, respectively, indicating a smaller spatial variability of $C_{nss-SO_4^{2-}}$ than that of C_{MBC} . This result implies that the concentrations of SO_4^{2-} in the lower troposphere were more uniform than those of BC in the Arctic regions we studied.

Regionally averaged TPW in Finland was higher than in both South Siberia and Alaska by factors of 3.1 and 2.4, respectively (Figure 14). SWE showed similar differences among these areas. The correlation between SWE and TPW near the snowpack sampling sites (Finland, Alaska, and South Siberia) is shown in Figure 15. For this correlation, we excluded data from Ny-Ålesund because of the strong altitude dependence of SWE (discussed in section 4.5). The SWE was well correlated with the TPW ($r^2 = 0.70$). The good correlation was also observed for the relationship between SWE and w at 925 hPa (Figure S12a). The w at 1,000 and

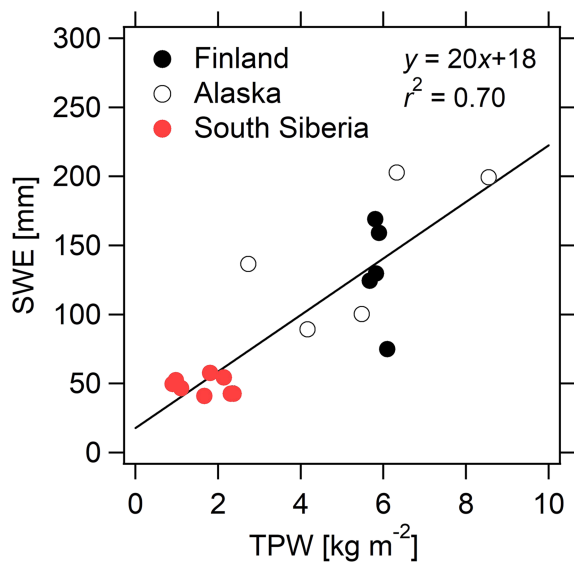


Figure 15. Correlation between SWE and TPW near snowpack sampling sites in Finland, Alaska, and South Siberia. The solid line indicates the least squares fitted regression.

in the air columns. Air parcels that reached the regions at high latitudes, distant from BC sources (northern Alaska, North Siberia, Greenland, and Ny-Ålesund), were more strongly influenced by wet removal of BC, leading to lower values of f_{600} and C_{MBC} there (Figure 16). Therefore, in addition to absolute values of C_{MBC} , correlations of f_{600} with C_{MBC} can provide important representations of BC removal by snowfall for use in assessments of climate models.

We estimated changes in the mass absorption cross section (MAC) of BC corresponding to the variability of the size distributions of BC (i.e., MMD and σ_{gm}) measured in this study. The size-dependent differential mass absorption cross section of BC reaches a maximum at a diameter of about 150 nm at a wavelength of 565 nm, calculated by Mie theory for a refractive index of $2.26 + 1.26i$ and density of 1.8 g/cm^3 (Kondo, 2015; Ohata et al., 2019). In this study, MMD varied from about 200 nm to about 360 nm and σ_{gm} varied from about 1.74 to about 2.25, as shown in Table 4. The corresponding change in MAC varied from 3.9 to $6.0 \text{ m}^2/\text{g}$ (about 40%).

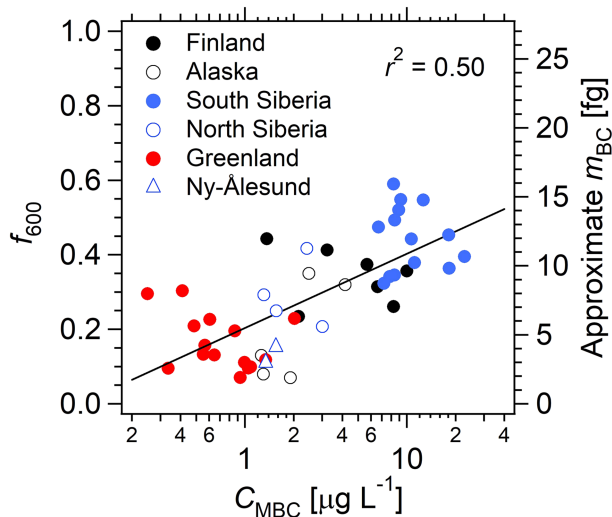


Figure 16. Correlation between f_{600} (m_{BC}) and C_{MBC} in the areas least influenced by local BC emissions. The solid line indicates the least squares fit for the relationship between f_{600} and C_{MBC} . Approximate m_{BC} was derived from the f_{600} - m_{BC} correlation in Figure A1.

925 hPa were highly correlated with saturation water vapor mixing ratio and temperature (Figures S12b and S12c). These relationships indicate that the temperature was an important factor in constraining SWE in the Arctic.

Regionally averaged DEP_{MBC} in Finland was higher than in Alaska because of the higher C_{MBC} in Finland. Regionally averaged DEP_{MBC} at Ny-Ålesund ($355 \pm 190 \text{ } \mu\text{g/m}^2$) was also somewhat higher than in Alaska ($234 \pm 138 \text{ } \mu\text{g/m}^2$) because of the much larger amounts of precipitation (equivalent to SWE) in Spitsbergen.

The distribution of regionally averaged $DEP_{nss-SO_4^{2-}}$ was more uniform than that of DEP_{MBC} , partly due to the more uniform distribution of $C_{nss-SO_4^{2-}}$ than that of C_{MBC} .

5.2. Size Distribution of BC

For the samples selected on the basis of low EF_{BC} , the correlation between f_{600} and C_{MBC} was moderately strong ($r^2 = 0.50$; Figure 16), but was stronger ($r^2 = 0.82$) for regionally averaged data (not shown). We suggest that in the regions of high C_{MBC} , the losses from air columns of BC particles with $D_{BC} > 600 \text{ nm}$ were lower because of the lower probability of their wet removal during transport from BC sources. Occasional snowfall events in these regions then efficiently remove any remaining large BC particles

in the air columns. Air parcels that reached the regions at high latitudes, distant from BC sources (northern Alaska, North Siberia, Greenland, and Ny-Ålesund), were more strongly influenced by wet removal of BC, leading to lower values of f_{600} and C_{MBC} there (Figure 16). Therefore, in addition to absolute values of C_{MBC} , correlations of f_{600} with C_{MBC} can provide important representations of BC removal by snowfall for use in assessments of climate models.

We estimated changes in the mass absorption cross section (MAC) of BC corresponding to the variability of the size distributions of BC (i.e., MMD and σ_{gm}) measured in this study. The size-dependent differential mass absorption cross section of BC reaches a maximum at a diameter of about 150 nm at a wavelength of 565 nm, calculated by Mie theory for a refractive index of $2.26 + 1.26i$ and density of 1.8 g/cm^3 (Kondo, 2015; Ohata et al., 2019). In this study, MMD varied from about 200 nm to about 360 nm and σ_{gm} varied from about 1.74 to about 2.25, as shown in Table 4. The corresponding change in MAC varied from 3.9 to $6.0 \text{ m}^2/\text{g}$ (about 40%).

6. Comparison With Previous BC Measurements

As described in section 1, ISSW analyses of C_{MBC} have been made over wide regions of the Arctic (Doherty et al., 2010) and the TOT technique has been used in some regions (Carmagnola et al., 2013; Forsström et al., 2013; Hagler et al., 2007; Meinander et al., 2013; Pedersen et al., 2015; Svensson et al., 2013). Previous studies have made direct comparisons of C_{MBC} measured by ISSW (C_{MBC} (ISSW)) and by TOT (C_{MBC} (TOT)) with those measured by the SP2/nebulizer system (C_{MBC} (SP2)) using the same samples (Lim et al., 2014; Schwarz et al., 2012). In this section, the uncertainties in the measurements of ISSW and TOT are described first. Then, we compare our C_{MBC} (SP2) values with the previous C_{MBC} (ISSW) and C_{MBC} (TOT) data at nearly the same locations or regions.

6.1. Uncertainties in ISSW Measurements of C_{MBC}

In section 1, we outlined the methodology and uncertainties of ISSW measurements of C_{MBC} . To elaborate, Schwarz et al. (2012) compared C_{MBC} (ISSW) with C_{MBC} (SP2) calibrated with fullerene soot. Their C_{MBC} (SP2) data were not influenced by light-scattering particles, including dust, as

is already well known (section 2.3). Schwarz et al. (2012) demonstrated that $C_{\text{MBC}}(\text{ISSW})/C_{\text{MBC}}(\text{SP2})$ ratios increased with increasing dust/BC and polystyrene latex (PSL)/BC mass concentration ratios by using dust- and PSL-contaminated samples. For dust/BC mass ratios of 30–120 and PSL/BC mass ratios of 10–450, $C_{\text{MBC}}(\text{ISSW})/C_{\text{MBC}}(\text{SP2})$ ratios ranged from 1 to 3 and from 2 to 5, respectively. Similarly, there can be large overestimates of $C_{\text{MBC}}(\text{ISSW})$ from field data, depending on dust/BC mass ratios. The differences in the optical properties of fullerene soot and ISSW calibration material (Monarch 71) can also cause overestimates of $C_{\text{MBC}}(\text{ISSW})$, depending on the assumed MAC and absorption Ångström exponents of BC (Schwarz et al., 2012). On the other hand, BC losses have occurred during filtration of samples (Doherty et al., 2010; Schwarz et al., 2012), which may have led to underestimates of $C_{\text{MBC}}(\text{ISSW})$.

6.2. Uncertainties in TOT Measurements of C_{MBC}

According to studies by Lim et al. (2014), the uncertainties of $C_{\text{MBC}}(\text{TOT})$ measurements are subtle. They reported both overestimations and underestimations of $C_{\text{MBC}}(\text{TOT})$, depending on the sample origin; their $C_{\text{MBC}}(\text{TOT})/C_{\text{MBC}}(\text{SP2})$ ratios ranged from 0.5 to 3.4. They attributed their underestimations of $C_{\text{MBC}}(\text{TOT})$ to the marked decrease with decreasing D_{BC} of the efficiency of the quartz fiber filters they used. They attributed overestimation of $C_{\text{MBC}}(\text{TOT})$ partly to pyrolyzation of organic carbon in samples of high organic carbon concentration. However, it is noteworthy that this type of interference is generally small for airborne aerosols in Asia (e.g., Kondo et al., 2009) and the Arctic (e.g., Sinha et al., 2017). We suggest that it is unclear whether the overestimates of $C_{\text{MBC}}(\text{TOT})$ by Lim et al. (2014) can be attributed to pyrolyzation of organic carbon.

6.3. Comparisons of C_{MBC} Measured by SP2, ISSW, and TOT

Here we compare the C_{MBC} data determined in this study ($C_{\text{MBC}}(\text{SP2})$) with $C_{\text{MBC}}(\text{ISSW})$ and $C_{\text{MBC}}(\text{TOT})$ obtained previously from Arctic snow samples (Table 5 and Figure 6), although the sampling times and locations were not exactly the same. The C_{MBC} data we chose for these comparisons were those least influenced by snowmelt, except for the snow samples from Sodankylä (Finland; Meinander et al., 2013). Our purpose is to investigate the consistency of the comparisons of the field data with the direct comparisons made in the laboratory studies of Schwarz et al. (2012) and Lim et al. (2014) discussed above (sections 6.1 and 6.2).

The $C_{\text{MBC}}(\text{ISSW})/C_{\text{MBC}}(\text{SP2})$ ratio for all samples included in the comparison ranged from 2.1 to 25 (average, 13.0) and was larger for lower $C_{\text{MBC}}(\text{SP2})$ values. For samples from Alaska and Greenland, $C_{\text{MBC}}(\text{ISSW})$ was larger than $C_{\text{MBC}}(\text{SP2})$ by about 4–9 $\mu\text{g/L}$. These differences far exceed the spatial and temporal variations of $C_{\text{MBC}}(\text{SP2})$ for each region and are qualitatively consistent with the results of Schwarz et al. (2012) described above.

$C_{\text{MBC}}(\text{TOT})/C_{\text{MBC}}(\text{SP2})$ ratios for Greenland data were less than 1. For the data from Finland measured by the Norwegian Polar Institute (NPI), the ratios were about 1.5, whereas those for data from Finland measured by the Finnish Meteorological Institute (FMI) ranged from 2.7 to 4.2 (average, 3.5). The differences between $C_{\text{MBC}}(\text{TOT})$ and $C_{\text{MBC}}(\text{SP2})$ for the FMI data were much larger than those for the NPI data. A plausible explanation for these differences is enhancement of C_{MBC} by the snowmelt for the FMI snow samples from Sodankylä (Meinander et al., 2013). For data from Spitsbergen, $C_{\text{MBC}}(\text{TOT})/C_{\text{MBC}}(\text{SP2})$ ratio was as high as 30. With the exception of the data from Spitsbergen, the $C_{\text{MBC}}(\text{TOT})/C_{\text{MBC}}(\text{SP2})$ ratios were within the variability observed by Lim et al. (2014).

The $C_{\text{MBC}}(\text{ISSW})$ data of Doherty et al. (2010) have previously been used to validate climate model calculations (Dou et al., 2012; Jiao et al., 2014; Lee et al., 2013). For Arctic data, despite the large uncertainties in estimates of $C_{\text{MBC}}(\text{ISSW})$, the correlation of $C_{\text{MBC}}(\text{ISSW})$ with C_{MBC} calculated by the GISS-E2PUCCINI-PUCCINI climate model (Dou & Xiao, 2016) was strong ($r^2 = 0.83$, slope = 0.75). This good agreement suggests that the climate model considerably overestimates C_{MBC} . This example clearly shows that the present $C_{\text{MBC}}(\text{SP2})$ data are very important for critical validation of the representation in climate models of wet deposition of BC over wide regions of the Arctic.

7. Summary and Conclusions

Improved understanding of the deposition of BC and inorganic aerosols in the Arctic is needed to assess the effects of aerosols on climate brought about by changes in snow albedo and the direct and indirect effects of

airborne particles. It is critically important to validate climate models by using observations of the key parameters relevant to aerosol deposition in Arctic snow: C_{MBC} , C_{NBC} , size distribution (f_{600}), SWE, and DEP_{MBC} for BC, and mass concentrations and DEP for inorganic ion species ($nss\text{-}SO_4^{2-}$, NO_3^- , Na^+ , and NH_4^+). Because few accurate measurements of these parameters are available, we used an SP2 to accurately measure their spatial distributions in snow samples collected before the snow melt season between 2012 and 2016 from Finland, Alaska, Siberia, Greenland, and Spitsbergen. We also compared our SP2 analyses with previous analyses of Arctic snow by the ISSW and TOT methods. The concentrations and amounts of inorganic aerosols deposited were interpreted on the basis of EF_{BC} , SWE, PBL thickness, three-day back trajectories, and topography.

In all of the Arctic regions we studied, average PBL heights during snow accumulation periods ranged from 0.2 to 1.1 km, depending on topography. Low PBL heights contributed to the accumulation of BC and other aerosols from local anthropogenic emission sources.

C_{MBC} and $C_{nss\text{-}SO_4^{2-}}$ were highest in samples from Finland and South Siberia, mainly related to high EF_{BC} in regions that are surrounded by mountains and hills, which promote accumulation of aerosols in the PBL. C_{MBC} and $C_{nss\text{-}SO_4^{2-}}$ were also high around large localized EF_{BC} sources at Anchorage and Fairbanks in Alaska. In contrast, C_{MBC} in samples from Alaska that were distant from cities was much lower due to the very low EF_{BC} in these areas. In Finland, both C_{MBC} and $C_{nss\text{-}SO_4^{2-}}$ decreased with increasing latitude north of $\sim 65^\circ N$ owing to weakening of the meridional flux of aerosols from lower latitudes, which in turn led to decreases in DEP_{MBC} and $DEP_{nss\text{-}SO_4^{2-}}$. C_{MBC} was well correlated with $C_{nss\text{-}SO_4^{2-}}$ in Finland. In northern Alaska, C_{MBC} showed a similar latitudinal dependence, but $C_{nss\text{-}SO_4^{2-}}$ was rather uniform because major sources of sulfate were more distant from the sampling areas.

In samples from Greenland, C_{MBC} depended little on altitude and its lateral distribution was largely uniform (average $0.81 \pm 0.46 \mu g/L$). Our analyses indicated that these aspects of the C_{MBC} distribution at Ny-Ålesund were similar to those in Greenland, thus indicating that the distributions of BC concentrations in the lower troposphere in winter and early spring are relatively uniform in these regions, which are distant from continental sources of anthropogenic BC.

SWE was generally well correlated with TPW near snow sampling sites. TPW was found to be an important factor in constraining SWE in the Arctic. The difference in the latitudinal variations of SWE between Finland and Alaska can be interpreted by the difference in TPW (or temperature) between the two regions.

Temperature in the lower troposphere generally decreased with increasing latitude, especially in winter and spring, indicating that air parcels during this period lost water vapor due to precipitation during transport from midlatitudes to the Arctic, thus leading to depositional loss of BC. Our analyses of C_{MBC} in each of the regions indicated that the observed latitudinal variations of C_{MBC} are a result of mixing and wet removal of BC during transport of air parcels from lower to higher latitudes. The latitudinal variation of $C_{nss\text{-}SO_4^{2-}}$ in these regions was considerably smaller than that of C_{MBC} , may be partly due to the effect of SO_4^{2-} formation during transport.

At locations of high C_{MBC} in South Siberia and Alaska, f_{600} was also high (~ 0.4), likely because airborne BC particles had not undergone sufficient wet removal to deplete the larger diameter BC particles. BC particles of $D_{BC} > 600$ nm remaining in the air parcels were then deposited onto snow, mainly by nucleation processes. In samples from Prudhoe Bay, f_{600} was relatively low (~ 0.26), suggesting that BC particles emitted by flaring of petroleum gas are smaller than those emitted in urban areas. For snow samples we collected, MMD varied from about 200 nm to about 360 nm and σ_{gm} varied from about 1.74 to about 2.25. The corresponding change in MAC was about 40%.

We compared our C_{MBC} values measured by an SP2 with those measured by the ISSW and TOT techniques for samples from Finland, Alaska, Spitsbergen, and Greenland, although the sampling locations and times are not exactly the same. The C_{MBC} values measured by ISSW were on average 13 times higher (range, 2.1 to 25) than those measured by SP2. The differences of our SP2 analyses from those obtained by the ISSW technique are qualitatively consistent with direct comparisons by Schwarz et al. (2012) and are much larger than the spatial variations of C_{MBC} measured by SP2 in these regions. The C_{MBC} measured by TOT was higher by a factor of 1.5 on average than those measured by SP2, for snow samples least influenced by

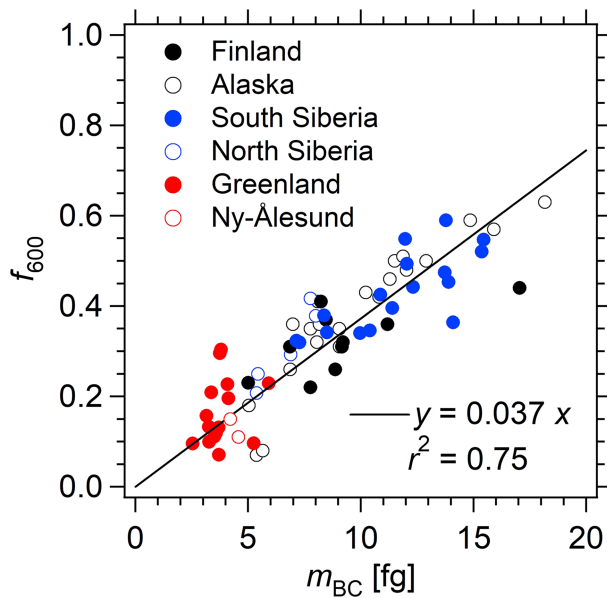


Figure A1. Correlation between f_{600} and m_{BC} for all snow samples. The solid line indicates the least squares fitted regression.

snowmelt. The differences of our SP2 analyses from those obtained by the TOT technique are also consistent with the direct comparisons by Lim et al. (2014). Our results clearly demonstrate the importance of the high-accuracy measurements of C_{MBC} , SWE, and DEP_{MBC} for constraining climate models that estimate the effects of BC on the Arctic climate.

Appendix A.

A1. Effects of Adhesion of BC on Surfaces of Glass Bottles and Plastic Bags

A1.1. a) Glass Bottles

As shown in section 2.4, C_{MBC} and C_{NBC} measured 42 months after melting snow samples were sufficiently reproducible. This result indicates that the effect of BC loss during storage in glass bottles is small.

A1.2. b) Plastic Bags

Most of snow samples were collected and melted in powder-free plastic bags, and some samples were transported to National Institute of Polar Research (NIPR) in Tokyo without being melted. A fraction of BC particles might have adhered to the inner surfaces of the bags. This possible loss of BC was evaluated.

We compared the C_{MBC} values of snow samples melted in their plastic sample bags with those measured without melting in the bags. Two sets of snow samples were collected from 14 depth-intervals in a snow pit dug at Ny-Ålesund in April 2013. First set of samples were melted and stirred in their bags and portions of melted samples were then transferred into precleaned glass bottles, which were then kept refrigerated at 4 °C until analysis. The second set of snow samples were collected in precleaned polyethylene bottles and transported to NIPR without being melted and were kept frozen at −30 °C until analysis. These samples were transferred to glass beakers and

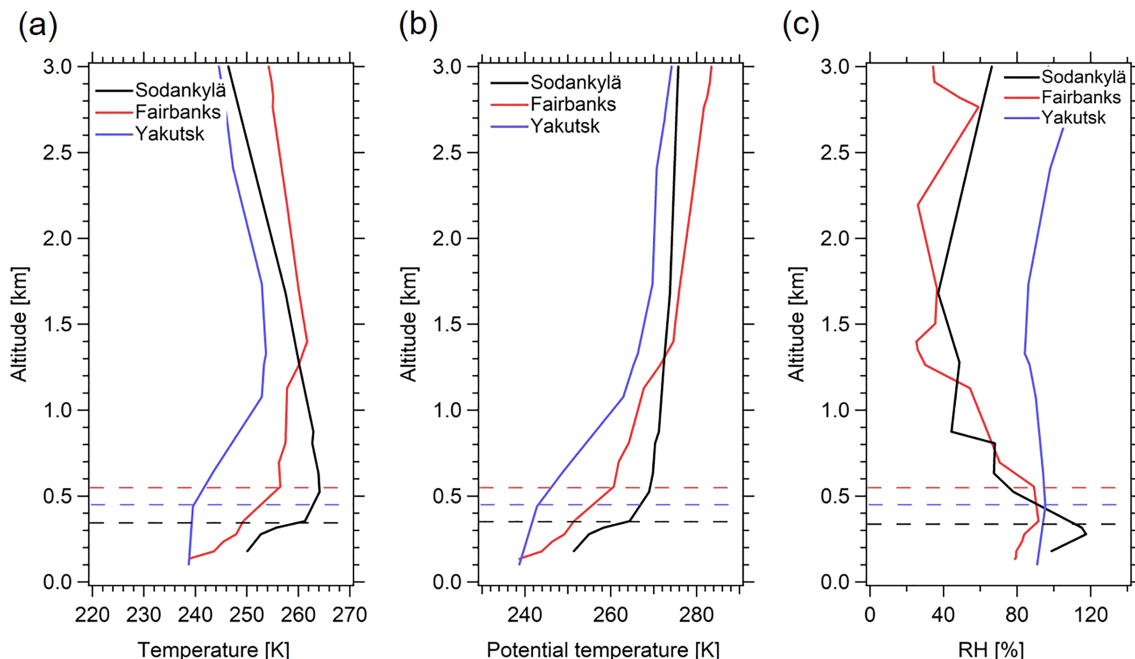


Figure A2. Vertical profiles of (a) temperature, (b) potential temperature, and (c) relative humidity (RH) at 1200 UTC in Sodankylä (26 January 2013), Fairbanks (1 December 2012), and Yakutsk (26 November 2012). Dashed lines indicate height of the PBL at each location as estimated from profiles of temperature and RH.

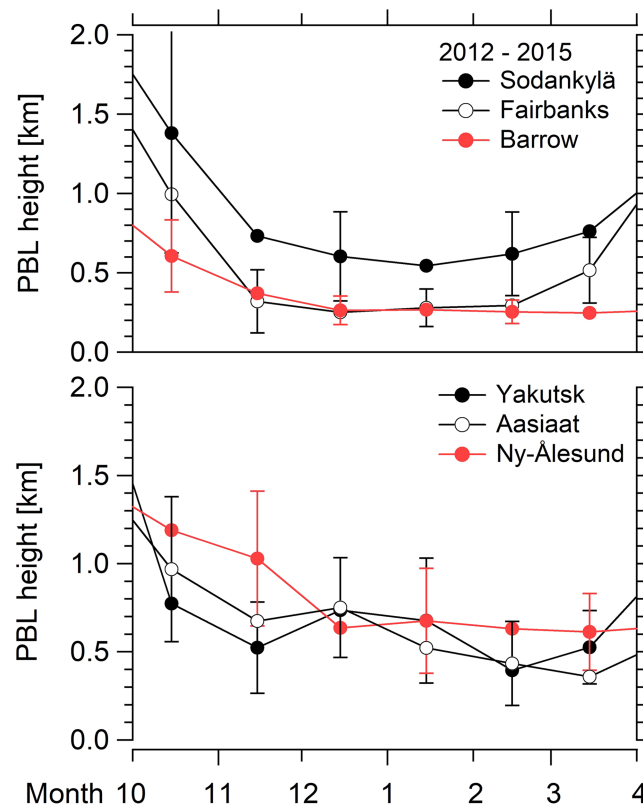


Figure A3. Monthly average PBL heights near snow sampling sites in Sodankylä, Fairbanks, Barrow, Yakutsk, Aasiaat in Greenland, and Ny-Ålesund in Spitsbergen during 2012–2015. Error bars indicate $\pm 1\sigma$.

melted in them before analysis. The C_{MBC} values of these two sets of samples agreed to within the uncertainty of the Marin-5/SP2 measurement. This result indicates that the effect of BC loss during storage in sample bags is small.

A2. Height of the Planetary Boundary Layer

We estimated the height of the PBL in Arctic regions by using profiles of temperature and RH obtained from the Integrated Global Radiosonde Archive, and then compared the heights of the PBL calculated by both the lapse rate (PBL_{Lap}) and bulk Richardson number (PBL_{Rib}) methods (Di Liberto et al., 2012; Garrett, 1981; Hayden et al., 1997). Detailed descriptions of these calculations are provided as below.

1. Lapse Rate Method

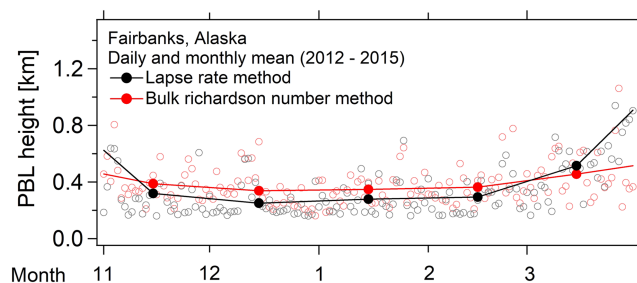


Figure A4. Daily and monthly means of PBL height in Fairbanks during the snow accumulation periods of 2012–2015 estimated by the lapse rate and bulk Richardson number methods.

Table 5
Comparisons of Previously Measured C_{MBC} in Surface Arctic Snow by the (a) ISSW (C_{MBC} (ISSW)) and (b) TOT (C_{MBC} (TOT)) Techniques With the SP2 (C_{MBC} (SP2)) Measurements of This Study in Samples From Similar Regions of the Arctic

(a)														
Region	Sampling sites	Previous study C_{MBC} (ISSW) ($\mu\text{g/L}$)			This study C_{MBC} (SP2) ($\mu\text{g/L}$)					Ratio	Institution	References		
		Average ($\pm 1\sigma$)	Median (25%, 75%)	Year	Average ($\pm 1\sigma$)	Median (25%, 75%)	Year	C_{MBC} (SP2) ($\mu\text{g/L}$)	C_{MBC} (ISSW) – C_{MBC} (SP2) ($\mu\text{g/L}$)					
Alaska	Barrow	9.0	9.0	2007	0.36	0.36	2013	8.6 (8.6)	25 (25)	UW	Doherty et al. (2010)			
Alaska	Whole area	12 \pm 8.5	9.0 (8.5, 10.5)	2007	5.6 \pm 5.3	3.7 (1.7, 7.2)	2012–2015	6.4 (5.3)	2.1 (2.4)	UW	Doherty et al. (2010)			
Greenland	Whole area	4.5 \pm 5.2	3.2 (1.8, 4.3)	2007, 2008	0.81 \pm 0.46	0.65 (0.52, 1.02)	2015–2016	3.7 (2.6)	5.6 (4.9)	UW	Doherty et al. (2010)			
Spitsbergen	Ny-Ålesund	13 \pm 4.7	15 (12, 16)	2007, 2009	0.70 \pm 0.38	0.70 (0.57, 0.83)	2013	12 (14)	19 (21)	UW	Doherty et al. (2010)			
(b)														
Region	Sampling sites	Previous study C_{MBC} (TOT) ($\mu\text{g/L}$)			This study C_{MBC} (SP2) ($\mu\text{g/L}$)					Ratio	Institution	References		
		Average ($\pm 1\sigma$)	Median (25%, 75%)	Year	Average ($\pm 1\sigma$)	Median (25%, 75%)	Year	C_{MBC} (TOT) – C_{MBC} (SP2) ($\mu\text{g/L}$)						
Finland	Sodankylä	35 \pm 23	25 (18, 47)	2010	8.3	8.3	2013	27 (17)	4.2 (3.0)	FMI	Meinander et al. (2013)			
Finland	Whole area	35 \pm 23	25 (18, 47)	2010	13 \pm 18	8.3 (4.5, 11)	2013	22 (17)	2.7 (3.0)	FMI	Meinander et al. (2013) and Svensson et al. (2013)			
Finland	Whole area	20 \pm 9	18 (15, 23)	2008, 2009	13 \pm 18	8.3 (4.5, 11)	2013	7 (10)	1.5 (2.2)	NPI	Forsström et al. (2013)			
Alaska	Barrow	8.9 \pm 0.2	8.8 (8.7, 8.9)	2008	5.6 \pm 5.3	3.7 (1.7, 7.2)	2013	3.3 (5.1)	1.6 (2.4)	NPI	Forsström et al. (2013) and Pedersen et al. (2015)			
Greenland	Whole area	0.3 \pm 0.3	-	2011	0.81 \pm 0.46	0.65 (0.52, 1.02)	2015–2016	-0.51 (-)	0.37 (-)	CEN	Carmagnola et al. (2013)			
Greenland	Whole area	0.56 \pm 0.40	0.41 (0.39, 0.60)	2002–2005	0.81 \pm 0.46	0.65 (0.52, 1.02)	2015–2016	-0.25 (-0.24)	0.69 (0.63)	Georgia Tech	Hagler et al. (2007)			
Spitsbergen	Ny-Ålesund	21 \pm 14	11 (10, 31)	2007–2011	0.70 \pm 0.38	0.70 (0.57, 0.83)	2013	20 (10)	30 (16)	NPI	Forsström et al. (2013) and Pedersen et al. (2015)			

Note. C_{MBC} (ISSW) was measured at the University of Washington (UW) in samples collected from Barrow in 2007, northern Alaska in 2007 (68°–70°N, 130°–140°W) about 200 km east of the region of our study, Greenland (61°–81°N, 20°–60°W) in 2007–2008, and Ny-Ålesund in 2007 and 2009. These snow samples did not undergo snowmelt. C_{MBC} (TOT) was measured from samples collected from Sodankylä in 2010, northern Finland (67°–69°N, 20°–25°E) in 2008–2010, Greenland (61°–81°N, 20°–60°W) in 2002–2005 and 2011, and Ny-Ålesund in 2007–2011 and was analyzed at the Finnish Meteorological Institute (FMI), Norwegian Polar Institute (NPI), French Snow Research Centre (CEN), and Georgia Institute of Technology (Georgia Tech, USA), respectively. Snowmelt had little influence on the measured C_{MBC} (TOT) values except for samples from Sodankylä in Finland (Meinander et al., 2013). Differences between C_{MBC} (SP2) and average (median) values of C_{MBC} (ISSW) and C_{MBC} (TOT) and the ratios of average (median) C_{MBC} (ISSW) and C_{MBC} (TOT) values to C_{MBC} (SP2) are also shown.

PBL_{Lap} is determined as the height that satisfies the following two conditions:

$$\frac{d\theta}{dz} > 2 \text{ [K/km]}, \quad (A1)$$

and

$$\frac{dRH}{dz} < 0 \text{ [%/km]}. \quad (A2)$$

where z and θ are altitude and potential temperature, respectively (Di Liberto et al., 2012; Hayden et al., 1997). Criterion (A1) has been shown to discriminate between the slightly positive lapse rate at the top of the PBL and stable air (Di Liberto et al., 2012; Garrett, 1981). Di Liberto et al. (2012) showed that PBL_{Lap} at Ny-Ålesund in summer agreed well with the PBL height obtained from lidar observations.

2. Bulk Richardson Number Method

Determinations of PBL_{Rib} use the bulk Richardson number (R_{ib}) defined as

$$R_{ib}(z) = g \frac{(z-z_0)[\theta(z)-\theta(z_0)]}{\theta(z)[u^2(z)-v^2(z)]}, \quad (A3)$$

where z is altitude (m), z_0 is ground altitude (m), g is gravitational acceleration (9.8 m/s^2), θ is potential temperature, and $u(z)$ and $v(z)$ are zonal and meridional components (m/s) of the wind vector, respectively. The numerator represents a buoyancy term associated with thermal production of turbulence, and the denominator represents wind shear associated with mechanical production of turbulence. PBL_{Rib} is defined as the height of the first level at which the critical value R_{ib} is greater than 0.21 (Di Liberto et al., 2012).

Examples of vertical profiles of temperature, θ , and RH in Sodankylä, Fairbanks, and Yakutsk show that the PBL_{Lap} is close to the upper boundary of the temperature inversion (Figure A2). More detailed analysis of the data from Fairbanks shows that this relationship holds statistically throughout winter and spring (data not shown). The height of the inversion layer is determined by turbulence in the surface layer and the energy balance between surface net radiation and atmospheric downwelling infrared radiation (Mayfield & Fochesatto, 2013; Overland & Guest, 1991; Seidel et al., 2010). Monthly averages of PBL_{Lap} from fall to early spring during 2012–2015 in Sodankylä, Fairbanks, Barrow, Yakutsk, Aasiaat in Greenland (68.7°N , 52.9°W ; 43 m asl), and Ny-Ålesund in Spitsbergen were generally lower than 700 m (Figure A3).

Daily and monthly averaged PBL_{Lap} and PBL_{Rib} in Fairbanks during the winters of 2012–2015 agreed to within 15% (Figure A4), thus giving a measure of the accuracy of our estimates of PBL height. However, the altitude resolutions of wind speed and direction data at some stations were too low for calculation of PBL_{Rib} . Therefore, we used PBL_{Lap} values for our analysis.

Acknowledgments

This work was supported by the Japanese Ministry of Education, Culture, Sports, Science, and Technology (MEXT); the Environment Research and Technology Development Fund (2-1403 and 2-1703) of the Environmental Restoration and Conservation Agency of Japan; the Japan Society for the Promotion of Science (JSPS) KAKENHI grants (JP12J06736, JP16J04452, JP23221001, JP23221004, JP26701004, JP26241003, JP16H01772, JP16H01770, JP18H03363, JP18H05292, and JP19K20441); the GRENE Arctic Climate Change Research Project; the Arctic Challenge for Sustainability (ArCS) project; and National Institute of Polar Research (Project Research KP-15). The data used in this study are available at <https://ads.nipr.ac.jp/dataset/A20190315-001>. We also used NOAA/NCEP Reanalysis data from <http://www.cdc.noaa.gov/>.

References

- Aamaas, B., Bøggild, C. E., Stordal, F., Berntsen, T., Holmén, K., & Ström, J. (2011). Elemental carbon deposition to Svalbard snow from Norwegian settlements and long-range transport. *Tellus Series B*, 63, 340–351. <https://doi.org/10.1111/j.1600-0889.2011.00531.x>
- Arctic Monitoring and Assessment Programme (AMAP) (2015). AMAP Assessment 2015: Black carbon and ozone as Arctic climate forcers (p. 116). Oslo, Norway. vii: Arctic Monitoring and Assessment Programme (AMAP). Retrieved from <http://www.amap.no/documents/doc/AMAP-Assessment-2015-Black-carbon-and-ozone-as-Arctic-climate-forcers/1299>
- Bolton, D. (1980). The computation of equivalent potential temperature. *Monthly Weather Review*, 108, 1046–1053. [https://doi.org/10.1175/1520-0493\(1980\)108<1046:TCOEPT>2.0.CO;2](https://doi.org/10.1175/1520-0493(1980)108<1046:TCOEPT>2.0.CO;2)
- Bond, T. C., Doherty, S. J., Fahey, D. W., Forster, P. M., Berntsen, T., DeAngelo, B. J., et al. (2013). Bounding the role of black carbon in the climate system: A scientific assessment. *Journal of Geophysical Research: Atmospheres*, 118, 5380–5552. <https://doi.org/10.1002/jgrd.50171>
- Brock, C. A., Cozic, J., Bahreini, R., Froyd, K. D., Middlebrook, A. M., McComiskey, A., et al. (2011). Characteristics, sources, and transport of aerosols measured in spring 2008 during the aerosol, radiation, and cloud processes affecting Arctic Climate (ARCPAC) Project. *Atmospheric Chemistry and Physics*, 11(6), 2423–2453. <https://doi.org/10.5194/acp-11-2423-2011>
- Browse, J., Carslaw, K. S., Arnold, S. R., Pringle, K., & Boucher, O. (2012). The scavenging processes controlling the seasonal cycle in the Arctic sulphate and black carbon aerosol. *Atmospheric Chemistry and Physics*, 12, 6775–6798. <https://doi.org/10.5194/acp-12-6775-2012>
- Carmagnola, C. M., Domine, F., Dumont, M., Wright, P., Strellis, B., Bergin, M., et al. (2013). Snow spectral albedo at Summit, Greenland: Measurements and numerical simulations based on physical and chemical properties of the snowpack. *The Cryosphere*, 7(4), 1139–1160. <https://doi.org/10.5194/tc-7-1139-2013>

- Di Liberto, L., Angelini, F., Pietroni, I., Cairo, F., Di Donfrancesco, G., Viola, A., et al. (2012). Estimate of the Arctic convective boundary layer height from lidar observations: A case study. *Advances in Meteorology*, 2012, 1–9. <https://doi.org/10.1155/2012/851927>
- Doherty, S. J., Hegg, D. A., Johnson, J. E., Quinn, P. K., Schwarz, J. P., Dang, C., & Warren, S. G. (2016). Causes of variability in light absorption by particles in snow at sites in Idaho and Utah. *Journal of Geophysical Research: Atmospheres*, 121, 4751–4768. <https://doi.org/10.1002/2015JD024375>
- Doherty, S. J., Warren, S. G., Grenfell, T. C., Clarke, A. D., & Brandt, R. E. (2010). Light-absorbing impurities in Arctic snow. *Atmospheric Chemistry and Physics*, 10, 11,647–11,680. <https://doi.org/10.5194/acp-10-11647-2010>
- Dou, T., Xiao, C., Shindell, D. T., Liu, J., Eleftheriadis, K., Ming, J., & Qin, D. (2012). The distribution of snow black carbon observed in the Arctic and compared to the GISS-PUCCINI model. *Atmospheric Chemistry and Physics*, 12, 7995–8007. <https://doi.org/10.5194/acp-12-7995-2012>
- Dou, T. F., & Xiao, C. D. (2016). An overview of black carbon deposition and its radiative forcing over the Arctic. *Advances in Climate Change Research*, 7, 115–122. <https://doi.org/10.1016/j.accre.2016.10.003>
- Douglas, T. A., & Sturm, M. (2004). Arctic haze, mercury and the chemical composition of snow across northwestern Alaska. *Atmospheric Environment*, 38, 805–820. <https://doi.org/10.1016/j.atmosenv.2003.10.042>
- Durre, I., Vose, R. S., & Wuertz, D. B. (2006). Overview of the integrated global radiosonde archive. *Journal of Climate*, 19, 53–68. <https://doi.org/10.1175/JCLI3594.1>
- Flanner, M. G., Zender, C. S., Randerson, J. T., & Rasch, P. J. (2007). Present-day climate forcing and response from black carbon in snow. *Journal of Geophysical Research*, 112, D11202. <https://doi.org/10.1029/2006JD008003>
- Førland, E. J., & Hanssen-Bauer, I. (2000). Increased precipitation in the Norwegian Arctic: True or false? *Climatic Change*, 46(4), 485–509. <https://doi.org/10.1023/A:1005613304674>
- Forsström, S., Isaksson, E., Skeie, R. B., Ström, J., Pedersen, C. A., Hudson, S. R., et al. (2013). Elemental carbon measurements in European Arctic snow packs. *Journal of Geophysical Research: Atmospheres*, 118, 13,614–13,627. <https://doi.org/10.1002/2013JD019886>
- Forsström, S., Ström, J., Pedersen, C. A., Isaksson, E., & Gerland, S. (2009). Elemental carbon distribution in Svalbard snow. *Journal of Geophysical Research*, 114, D19112. <https://doi.org/10.1029/2008JD011480>
- Garrett, A. J. (1981). Comparison of observed mixed-layer depths to model estimates using observed temperatures and winds, and MOS forecasts. *Journal of Applied Meteorological and Climatology*, 20, 1277–1283.
- Goto-Azuma, K., Hirabayashi, M., Motoyama, H., Miyake, T., Kuramoto, T., Uemura, R., et al. (2019). Reduced marine phytoplankton sulphur emissions in the Southern Ocean during the past seven glacial. *Nature Communications*, 10(1), 3247. <https://doi.org/10.1038/s41467-019-11128-6>
- Hadley, O. L., & Kirchstetter, T. W. (2012). Black-carbon reduction of snow albedo. *Nature Climate Change*, 2, 437–440. <https://doi.org/10.1038/nclimate1433>
- Hagler, G. S. W., Bergin, M. H., Smith, E. A., Dibb, J. E., Anderson, C., & Steig, E. J. (2007). Particulate and water-soluble carbon measured in recent snow at Summit, Greenland. *Geophysical Research Letters*, 34, L16505. <https://doi.org/10.1029/2007GL030110>
- Hayden, K. L., Anlauf, K. G., Hoff, R. M., Strapp, J. W., Bottenheim, J. W., Wiebe, H. A., et al. (1997). The vertical chemical and meteorological structure of the boundary layer in the Lower Fraser Valley during Pacific '93. *Atmospheric Environment*, 31(14), 2089–2105. [https://doi.org/10.1016/S1352-2310\(96\)00300-7](https://doi.org/10.1016/S1352-2310(96)00300-7)
- Huang, L., Gong, S. L., Sharma, S., Lavoué, D., & Jia, C. Q. (2010). A trajectory analysis of atmospheric transport of black carbon aerosols to Canadian high Arctic in winter and spring (1990–2005). *Atmospheric Chemistry and Physics*, 10(11), 5065–5073. <https://doi.org/10.5194/acp-10-5065-2010>
- Intergovernmental Panel on Climate Change (2013). *The Physical Science Basis, Contribution of Working Group I to the Fourth Assessment Report of the Intergovernmental Panel on Climate Change*. Cambridge, UK: Cambridge University Press.
- Irannezhad, M., Marttila, H., & Kløve, B. (2014). Long-term variations and trends in precipitation in Finland. *International Journal of Climatology*, 34, 3139–3153. <https://doi.org/10.1002/joc.3902>
- Jiao, C., Flanner, M. G., Balkanski, Y., Bauer, S. E., Ballouin, N., Bernsten, T. K., et al. (2014). An AeroCom assessment of black carbon in Arctic snow and sea ice. *Atmospheric Chemistry and Physics*, 14(5), 2399–2417. <https://doi.org/10.5194/acp-14-2399-2014>
- Kaspari, S., Schwikowski, M., Gysel, M., Flanner, M. G., Kang, S., Hou, S., & Mayewski, P. A. (2011). Recent increase in black carbon concentrations from a Mt. Everest ice core spanning 1860–2000 AD. *Geophysical Research Letters*, 38, L04703. <https://doi.org/10.1029/2010GL046096>
- Katich, J. M., Perring, A. E., & Schwarz, J. P. (2017). Optimized detection of particulates from liquid samples in the aerosol phase: Focus on black carbon. *Aerosol Science and Technology*, 51(5), 543–553. <https://doi.org/10.1080/02786826.2017.1280597>
- Keene, W. C., Pszenny, A. A. P., Galloway, J. N., & Hawley, M. E. (1986). Sea-salt corrections and interpretation of constituent ratios in marine precipitation. *Journal of Geophysical Research*, 91, 6647–6657. <https://doi.org/10.1029/JD091iD06p06647>
- Khan, A. L., Dierssen, H., Schwarz, J. P., Schmitt, C., Chlus, A., Hermanson, M., et al. (2017). Impacts of coal dust from an active mine on the spectral reflectance of Arctic surface snow in Svalbard, Norway. *Journal of Geophysical Research: Atmospheres*, 122, 1767–1778. <https://doi.org/10.1002/2016JD025757>
- Kondo, Y. (2015). Effects of black carbon on climate: Advances in measurement and modeling. *Monographs on Environment, Earth and Planets*, 3, 1–85. <https://doi.org/10.5047/meep.2015.00301.0001>
- Kondo, Y., Moteki, N., Oshima, N., Ohata, S., Koike, M., Shibano, Y., et al. (2016). Effects of wet deposition on the abundance and size distribution of black carbon in East Asia. *Journal of Geophysical Research: Atmospheres*, 121, 4691–4712. <https://doi.org/10.1002/2015JD024479>
- Kondo, Y., Sahu, L., Kuwata, M., Miyazaki, Y., Takegawa, N., Moteki, N., et al. (2009). Stabilization of the mass absorption cross section of black carbon for filter-based absorption photometry by the use of a heated inlet. *Aerosol Science and Technology*, 43(8), 741–756. <https://doi.org/10.1080/02786820902889879>
- Lamarque, J.-F., Bond, T. C., Eyring, V., Granier, C., Heil, A., Klimont, Z., et al. (2010). Historical (1850–2000) gridded anthropogenic and biomass burning emissions of reactive gases and aerosols: methodology and application. *Atmospheric Chemistry and Physics*, 10(15), 7017–7039. <https://doi.org/10.5194/acp-10-7017-2010>
- Lee, Y. H., Lamarque, J.-F., Flanner, M. G., Jiao, C., Shindell, D. T., Bernsten, T., et al. (2013). Evaluation of preindustrial to present-day black carbon and its albedo forcing from atmospheric chemistry and climate model intercomparison project (ACCMIP). *Atmospheric Chemistry and Physics*, 13(5), 2607–2634. <https://doi.org/10.5194/acp-13-2607-2013>
- Leeper, R. D., Palecki, M. A., & Davis, E. (2015). Methods to calculate precipitation from weighing-bucket gauges with redundant depth measurements. *Journal of Atmospheric and Oceanic Technology*, 32, 1179–1190. <https://doi.org/10.1175/JTECH-D-14-00185.1>

- Lim, S., Faïn, X., Zanatta, M., Cozic, J., Jaffrezo, J.-L., Ginot, P., & Laj, P. (2014). Refractory black carbon mass concentrations in snow and ice: Method evaluation and inter-comparison with elemental carbon measurement. *Atmospheric Measurement Techniques*, 7, 3307–3324. <https://doi.org/10.5194/amt-7-3307-2014>
- Liu, D., Quennehen, B., Darbyshire, E., Allan, J. D., Williams, P. I., Taylor, J. W., et al. (2015). The importance of Asia as a source of black carbon to the European Arctic during springtime 2013. *Atmospheric Chemistry and Physics*, 15(20), 11,537–11,555. <https://doi.org/10.5194/acp-15-11537-2015>
- Lohmann, U., & Feichter, J. (2005). Global indirect aerosol effect: a review. *Atmospheric Chemistry and Physics*, 5, 715–737. <https://doi.org/10.5194/acp-5-715-2005>
- Macdonald, K. M., Sharma, S., Toom, D., Chivulescu, A., Hanna, S., Bertram, A. K., et al. (2017). Observations of atmospheric chemical deposition to high Arctic snow. *Atmospheric Chemistry and Physics*, 17(9), 5775–5788. <https://doi.org/10.5194/acp-17-5775-2017>
- Mayfield, J. A., & Fochesatto, G. J. (2013). The layered structure of the winter atmospheric boundary layer in the interior of Alaska. *Journal of Applied Meteorology and Climatology*, 52, 953–973. <https://doi.org/10.1175/JAMC-D-12-01.1>
- McConnell, J. R., Edwards, R., Kok, G. L., Flanner, M. G., Zender, C. S., Saltzman, E. S., et al. (2007). 20th-century industrial black carbon emissions altered Arctic climate forcing. *Science*, 317(5843), 1381–1384. <https://doi.org/10.1126/science.1144856>
- Meinander, O., Kazadzis, S., Arola, A., Riihelä, A., Räisänen, P., Kivi, R., et al. (2013). Spectral albedo of seasonal snow during intensive melt period at Sodankylä, beyond the Arctic Circle. *Atmospheric Chemistry and Physics*, 13(7), 3793–3810. <https://doi.org/10.5194/acp-13-3793-2013>
- Mori, T., Kondo, Y., Ohata, S., Moteki, N., Matsui, H., Oshima, N., & Iwasaki, A. (2014). Wet deposition of black carbon at a remote site in the East China Sea. *Journal of Geophysical Research: Atmospheres*, 119, 10,485–10,498. <https://doi.org/10.1002/2014JD022103>
- Mori, T., Moteki, N., Ohata, S., Koike, M., Goto-Azuma, K., Miyazaki, Y., & Kondo, Y. (2016). Improved technique for measuring the size distribution of black carbon particles in liquid water. *Aerosol Science and Technology*, 50(3), 242–254. <https://doi.org/10.1080/02786826.2016.1147644>
- Moteki, N., & Kondo, Y. (2010). Dependence of laser-induced incandescence on physical properties of black carbon aerosols: Measurements and theoretical interpretation. *Aerosol Science and Technology*, 44, 663–675. <https://doi.org/10.1080/02786826.2010.484450>
- Moteki, N., Kondo, Y., & Nakamura, S. (2010). Method to measure refractive indices of small nonspherical particles: Application to black carbon particles. *Journal of Aerosol Science*, 41(5), 513–521. <https://doi.org/10.1016/j.jaerosci.2010.02.013>
- Moteki, N., Kondo, Y., Oshima, N., Takegawa, N., Koike, M., Kita, K., et al. (2012). Size dependence of wet removal of black carbon aerosols during transport from the boundary layer to the free troposphere. *Geophysical Research Letters*, 39, L13802. <https://doi.org/10.1029/2012GL052034>
- Moteki, N., & Mori, T. (2015). Theoretical analysis of a method to measure size distributions of solid particles in water by aerosolization. *Journal of Aerosol Science*, 83, 25–31. <https://doi.org/10.1016/j.jaerosci.2015.02.002>
- Moteki, N., Mori, T., Matsui, H., & Ohata, S. (2019). Observational constraint of in-cloud supersaturation for simulations of aerosol rainout in atmospheric models. *npj Climate and Atmospheric Science*, 2(1), 1–11. <https://doi.org/10.1038/s41612-019-0063-y>
- Murakami, M., Magono, C., & Kikuchi, K. (1985). Experiments on aerosol scavenging by natural snow crystals, Part III: The effect of snow crystal charge on collection efficiency. *Journal of the Meteorological Society of Japan*, 63(6), 1127–1137. https://doi.org/10.2151/jmsj1965.63.6_1127
- Murphy, D. M., & Koop, T. (2005). Review of the vapour pressures of ice and supercooled water for atmospheric applications. *Quarterly Journal of the Royal Meteorological Society*, 131(608), 1539–1565. <https://doi.org/10.1256/qj.04.94>
- Ohata, S., Kondo, Y., Moteki, N., Mori, T., Yoshida, A., Sinha, P. R., & Koike, M. (2019). Accuracy of black carbon measurements by a filter-based absorption photometer with a heated inlet. *Aerosol Science and Technology*. <https://doi.org/10.1080/02786826.2019.1627283>
- Ohata, S., Moteki, N., Mori, T., Koike, M., & Kondo, Y. (2016). A key process controlling the wet removal of aerosols: new observational evidence. *Nature Scientific Reports*, 6, 34113. <https://doi.org/10.1038/srep34113>
- Overland, J. E., & Guest, P. S. (1991). The Arctic snow and air temperature budget over sea ice during winter. *Journal of Geophysical Research*, 96, 4651–4662. <https://doi.org/10.1029/90JC02264>
- Pedersen, C. A., Gallet, J.-C., Ström, J., Gerland, S., Hudson, S. R., Forsström, S., et al. (2015). In situ observations of black carbon in snow and the corresponding spectral surface albedo reduction. *Journal of Geophysical Research: Atmospheres*, 120, 1476–1489. <https://doi.org/10.1002/2014JD022407>
- Raidla, V., Kaup, E., & Ivask, J. (2015). Factors affecting the chemical composition of snowpack in the Kilpisjärvi area of North Scandinavia. *Atmospheric Environment*, 118, 211–218. <https://doi.org/10.1016/j.atmosenv.2015.07.043>
- Rémy, S., Veira, A., Paugam, R., Sofiev, M., Kaiser, J. W., Marengo, F., et al. (2017). Two global data sets of daily fire emission injection heights since 2003. *Atmospheric Chemistry and Physics*, 17(4), 2921–2942. <https://doi.org/10.5194/acp-17-2921-2017>
- Schwarz, J. P., Doherty, S. J., Li, F., Ruggiero, S. T., Tanner, C. E., Perring, A. E., et al. (2012). Assessing single particle soot photometer and integrating sphere/integrating sandwich spectrophotometer measurement techniques for quantifying black carbon concentration in snow. *Atmospheric Measurement Techniques*, 5(11), 2581–2592. <https://doi.org/10.5194/amt-5-2581-2012>
- Schwarz, J. P., Gao, R. S., Spackman, J. R., Watts, L. A., Thomson, D. S., Fahey, D. W., et al. (2008). Measurement of the mixing state, mass, and optical size of individual black carbon particles in urban and biomass burning emissions. *Geophysical Research Letters*, 35, L13810. <https://doi.org/10.1029/2008GL033968>
- Seidel, D. J., Ao, C. O., & Li, K. (2010). Estimating climatological planetary boundary layer heights from radiosonde observations: Comparison of methods and uncertainty analysis. *Journal of Geophysical Research*, 115, D16113. <https://doi.org/10.1029/2009JD013680>
- Sinha, P. R., Kondo, Y., Goto-Azuma, K., Tsukagawa, Y., Fukuda, K., Koike, M., et al. (2018). Seasonal progression of the deposition of black carbon by snowfall at Ny-Ålesund, Spitsbergen. *Journal of Geophysical Research: Atmospheres*, 123, 997–1016. <https://doi.org/10.1002/2017JD028027>
- Sinha, P. R., Kondo, Y., Koike, M., Ogren, J. A., Jefferson, A., Barrett, T. E., et al. (2017). Evaluation of ground-based black carbon measurements by filter-based photometers at two Arctic sites. *Journal of Geophysical Research: Atmospheres*, 122, 3544–3572. <https://doi.org/10.1002/2016JD025843>
- Steffen, K., & Box, J. E. (2001). Surface climatology of the Greenland ice sheet: Greenland climate network 1995–1999. *Journal of Geophysical Research*, 106(D24), 33,951–33,964. <https://doi.org/10.1029/2001JD000161>
- Stohl, A., Klimont, Z., Eckhardt, S., Kupiainen, K., Shevchenko, V. P., Kopeikin, V. M., & Novigatsky, A. N. (2013). Black carbon in the Arctic: the underestimated role of gas flaring and residential combustion emissions. *Atmospheric Chemistry and Physics*, 13, 8833–8855. <https://doi.org/10.5194/acp-13-8833-2013>

- Svensson, J., Ström, J., Hansson, M., Lihavainen, H., & Kerminen, V.-M. (2013). Observed metre scale horizontal variability of elemental carbon in surface snow. *Environmental Research Letters*, 8(3), 034012. <https://doi.org/10.1088/1748-9326/8/3/034012>
- Taskinen, A., & Söderholm, K. (2016). Operational correction of daily precipitation measurements in Finland. *Boreal Environment Research*, 21, 1–24.
- Tollefson, J. (2009). Climate's smoky spectre. *Nature*, 460(7251), 29–32. <https://doi.org/10.1038/460029a>
- Tran, H. N. Q., & Mölders, N. (2011). Investigations on meteorological conditions for elevated PM_{2.5} in Fairbanks, Alaska. *Atmospheric Research*, 99, 39–49. <https://doi.org/10.1016/j.atmosres.2010.08.028>
- Tran, T. T., Newby, G., & Mölders, N. (2011). Impacts of emission changes on sulfate aerosols in Alaska. *Atmospheric Environment*, 45, 3078–3090. <https://doi.org/10.1016/j.atmosenv.2011.03.013>
- Wang, Y., & Hopke, P. K. (2014). Is Alaska truly the great escape from air pollution? - Long term source apportionment of fine particulate matter in Fairbanks, Alaska. *Aerosol and Air Quality Research*, 14(7), 1875–1882. <https://doi.org/10.4209/aaqr.2014.03.0047>
- Ward, T., Trost, B., Conner, J., Flanagan, J., & Jayanty, R. K. M. (2012). Source apportionment of PM_{2.5} in a subarctic airshed — Fairbanks, Alaska. *Aerosol and Air Quality Research*, 12, 536–543. <https://doi.org/10.4209/aaqr.2011.11.0208>
- Wendl, I. A., Menking, J. A., Färber, R., Gysel, M., Kaspari, S. D., Laborde, M. J. G., & Schwikowski, M. (2014). Optimized method for black carbon analysis in ice and snow using the Single Particle Soot Photometer. *Atmospheric Measurement Techniques*, 7, 2667–2681. <https://doi.org/10.5194/amt-7-2667-2014>
- Wright, R. F., & Dovland, H. (1978). Regional surveys of the chemistry of the snowpack in Norway, late winter 1973, 1974, 1975 and 1976. *Atmospheric Environment*, 12, 1755–1768. [https://doi.org/10.1016/0004-6981\(78\)90324-4](https://doi.org/10.1016/0004-6981(78)90324-4)
- Yang, Y., Wang, H., Smith, S. J., Easter, R. C., & Rasch, P. J. (2018). Sulfate aerosol in the Arctic: Source attribution and radiative forcing. *Journal of Geophysical Research: Atmospheres*, 123, 1899–1918. <https://doi.org/10.1002/2017JD027298>
- Yoshida, A., Moteki, N., Ohata, S., Mori, T., Tada, R., Dagsson-Waldhauserová, P., & Kondo, Y. (2016). Detection of light-absorbing iron oxide particles using a modified single-particle soot photometer. *Aerosol Science and Technology*, 50(3), 1–4. <https://doi.org/10.1080/02786826.2016.1146402>
- Yu, H., Kaufman, Y. J., Chin, M., Feingold, G., Remer, L. A., Anderson, T. L., et al. (2006). A review of measurement-based assessments of the aerosol direct radiative effect and forcing. *Atmospheric Chemistry and Physics*, 6(3), 613–666. <https://doi.org/10.5194/acp-6-613-2006>
- Zhang, L., Wang, X., Moran, M. D., & Feng, J. (2013). Review and uncertainty assessment of size-resolved scavenging coefficient formulations for below-cloud snow scavenging of atmospheric aerosols. *Atmospheric Chemistry and Physics*, 13, 10,005–10,025. <https://doi.org/10.5194/acp-13-10005-2013>